Numerical Modeling of RC Slabs on Tensionless Elastic Subgrade

by

Mansoor Ali Beg

A Thesis Presented to the

FACULTY OF THE COLLEGE OF GRADUATE STUDIES

KING FAHD UNIVERSITY OF PETROLEUM & MINERALS

DHAHRAN, SAUDI ARABIA

In Partial Fulfillment of the
Requirements for the Degree of

MASTER OF SCIENCE

In

CIVIL ENGINEERING

July, 1996

Numerical Modeling of RC Slabs on Tensionless Elastic Subgrade

BY

Mansoor Ali Beg

A Thesis Presented to the

FACULTY OF THE COLLEGE OF GRADUATE STUDIES

KING FAHD UNIVERSITY OF PETROLEUM & MINERALS

DHAHRAN, SAUDI ARABIA

In Partial Fulfillment of the
Requirements for the Degree of

MASTER OF SCIENCE

In

Civil Engineering

July 1996

KING FAHD UNIVERSITY OF PETROLEUM AND MINERALS
DHAHRAN 31261, SAUDI ARABIA

COLLEGE OF GRADUATE STUDIES

This thesis, written by **Mansoor Ali Beg** under the direction of his Thesis Advisor and approved by his Thesis committee, has been presented to and accepted by the Dean, College of Graduate Studies, in partial fulfillment of the requirements for the degree of

MASTER OF SCIENCE IN CIVIL ENGINEERING

Thesis Committee:

Dr.Abdul Rehman Al-Khathlan (*Thesis Advisor*)

Dr. Sajid Ali Abbasi (*Member*)

Dr. Naser Abdulrahman Al-Shayea (*Member*)

Dr. Abdullah A. Al-Musallam (*Member*)

Dr. Alfarabi Sharif
(*Department Chairman*)

Dr. Ala H. Al-Rabeh
(*Dean, College of Graduate Studies*)

12 th Aug. '96
Date

Dedicated to

my parents

Acknowledgment

In the name of Allah, Most Gracious, Most Merciful. Read in the name of thy Lord and Cherisher, Who created. Created man from a {leech-like} clot. Read and thy Lord is Most Bountiful. He Who taught {the use of} the pen. Taught man that which he knew not. Nay, but man doth transgress all bounds. In that he looketh upon himself as self-sufficient. Verily, to they Lord is the return {of all}.

(The Holy Quran, Surah 96)

First and foremost, all praise to the Almighty Allah Who gave me the courage and patience to carry out this work.

Acknowledgment is due to King Fahd University of Petroleum and Minerals for providing support to this work.

My deep appreciation goes to my thesis advisor Dr. Khathlan for his constant help, guidance and the attention that he devoted throughout the course of this work. I thank him for his priceless suggestions which made this work interesting and learning for me.

Thanks are also due to my thesis committee members Dr. Naser Al-Shayea, Dr. Sajid Ali Abbasi, and Dr. Abdullah Al-Musallam for their interest, cooperation, advice and constructive criticism.

I would like to thank my parents whose constant efforts, encouragement, and hard work made it possible for me to reach this stage in life.

My stay in KFUPM was made more fun by staying with friends in campus. Special thanks are due to my special friends at line 730. Atif, Ibrahim, Ashiq Sahab, Sabih and Saleem.

Contents

Acknowledgement i

List of Figures vi

List of Tables x

Abstract (English) xi

Abstract (Arabic) xii

1 INTRODUCTION 1

1.1 General 1

1.2 Slabs-on-Grade 2

1.3 Numerical Methods for Slabs-on-Grade 3

1.4 Subgrade Models 4

1.5 Problem Definition 5

1.6 Objectives 6

2 LITERATURE REVIEW 7

2.1 Reinforced Concrete Slabs 7

2.2 Slabs-on-Grade 10

3 NON-LINEAR FINITE ELEMENT MODELING OF RC SLABS 17

3.1 Material Modeling 18

3.1.1 Behavior of Concrete 18

3.1.2 Behavior of Steel 21

3.2 Finite Element Model 23

3.2.1 Element Description 23

3.2.2 Slab Element Stiffness Matrix 25

3.2.3 Numerical Integration 25

3.2.4 Layered Approach 26

3.2.5 Finite Element Solution 26

4 WINKLER SUBGRADE MODELING 31

4.1 Description 31

4.2 Loss of Contact Problem 33

4.3 Methodology for Modeling 33

4.4 Finite Element Formulation 35

5 PSUEDO-3D SUBGRADE MODEL 38

5.1 Description 38

5.2 Methodology of Modeling 39

5.3 Three Dimensional Element 42

5.4 Finite Element Formulation 42

6 NUMERICAL ASPECTS AND PROGRAM DESCRIPTION 47

6.1 Introduction 47

6.2 Program WINKLER 48

6.2.1 Material and Finite Element Parameters 48

6.2.2 Main Data Variables 50

6.2.3 Sequential Operation 51

6.2.4 Subroutines 51

6.3 Program PSUEDO-3D 57

6.3.1 Material and Finite Element Parameters 57

6.3.2 Evaluation of the Equivalent Subgrade Modulus 58

6.3.3 Sequential Operation 59

6.3.4 Subroutines 59

7 RESULTS AND DISCUSSIONS 64

7.1 Problem Description 64

7.2 Verification of the Model 66

7.2.1 Elastic Behavior 66

7.2.2 Inelastic Behavior 68

7.3 Winkler Model - Cavity Effect 70

7.3.1 Effect of Cavity Size 70

7.3.2 Effect of Cavity Location 75

7.4 PSEUDO-3D Model - Elastic Analysis 84

7.4.1 Geometry Description 84

7.4.2 Comparison of PSEUDO-3D and WINKLER Model 86

7.4.3 Convergence Phenomenon 88

7.4.4 Elastic Deformations 90

7.4.5 Equivalent Subgrade Modulus 96

7.5 Inelastic Analysis using PSEUDO-3D 101

7.5.1 Case Description 101

7.5.2 Non-linear Behavior 101

7.5.3 Equivalent Subgrade Modulus 106

8 SUMMARY, CONCLUSIONS AND RECOMMENDATIONS 110

8.1 Summary 110

8.2 Conclusions 111

8.3 Recommendations for future studies 114

Bibliography 114

Vita 120

List of Figures

3.1 Uniaxial Compressive Stress-Strain Curve for Concrete. 19

3.2 Tension-stiffening Behavior in Cracked Concrete. 22

3.3 Nodal Configuration of 9-noded Lagrangian Element. 24

3.4 Layered Element Model for Reinforced Concrete Slab. 27

5.1 Nodal Configuration of Three Dimensional Hexahedral Element. . . . 43

6.1 Flowchart for the WINKLER Model (contd...) 52

6.2 Flowchart for the PSEUDO-3D Model (contd...) 60

7.1 Square R/C Slab on Subgrade with Central Patch Load. 65

7.2 Comparison of Size of Contact Zone Dependence on the Relative Stiffness, λ. 67

7.3 Load - Central Deflection Curve in Comparison to Richart's Experimental Failure Load and ACI. 69

7.4 Four Cavities considered for the Cavity Size Effect Study. 71

7.5 Load - Central Deflection (Point A) Curves for a Slab with Cavities I, II, III & IV and without a Cavity. 73

7.6 Load - Corner Deflection (Point B) Curves for a Slab with Cavities I, II, III & IV and without a Cavity. 74

7.7 Type of Cavities Considered for the Cavity Location Effect Study. . . 77

7.8 Load - Central Deflection (Point A) Curves for a Slab with Cavities I, II, & III and with $k = 0.01kN/cm^3$. 78

7.9 Load - Central Deflection (Point A) Curves for a Slab with Cavities I, II, & III and with $k = 0.1kN/cm^3$. 79

7.10 Load - Corner Deflection (Point B) Curves for a Slab with Cavities I, II, & III and with $k = 0.01kN/cm^3$. 80

7.11 Load - Corner Deflection (Point B) Curves for a Slab with Cavities I, II, & III and with $k = 0.1kN/cm^3$. 81

7.12 Displacement Profile along X-axis for a Slab with Cavities I,II, & III at the Ultimate Loads of each and with $k = 0.01kN/cm^3$. 82

7.13 Displacement Profile along X-axis for a Slab with cavities I,II, & III at the Ultimate Loads of each and with $k = 0.1kN/cm^3$. 83

7.14 Quarter Model of Slab on a Three Dimensional Elastic Soil. 85

7.15 Comparison of Results of PSEUDO-3D Model and WINKLER Model. 87

7.16 Convergence Sequence of the Slab Displacements and Soil Displacement for Different Iterations. 89

7.17 Displacement Profile for a Slab Subjected to Patch Loading on a Soft Soil ($\overline{\lambda} = 1.675$). 91

7.18 Displacement Profile for a Slab Subjected to Uniformly Distributed Load on a Stiff Soil ($\overline{\lambda} = 1675$). 92

7.19 Displacement Profile for a Slab Subjected to Patch Loading on an Intermediate Soil ($\overline{\lambda} = 16.75$). 93

7.20 Displacement Profile for a Slab Subjected to Patch Loading on a Stiff Soil ($\overline{\lambda} = 1675$). 94

7.21 Schematic Comparison of Displacement Profiles obtained by Winkler (b). Pseudo-3d (c) and a Full-3d (d) Models. 95

7.22 Contours of dimensionless relative stiffness parameter α for a slab subjected to patch loading on a weak soil ($\overline{\lambda} = 1.675$). 97

7.23 Contours of dimensionless relative stiffness parameter α for a slab subjected to uniformly distributed load on a stiff soil ($\overline{\lambda} = 1675$). . . . 98

7.24 Contours of dimensionless relative stiffness parameter α for a slab subjected to patch loading on an intermediate soil ($\overline{\lambda} = 16.75$). 99

7.25 Contours of dimensionless relative stiffness parameter α for a slab subjected to patch loading on a stiff soil ($\overline{\lambda} = 1675$). 100

7.26 Load - Central Deflection Curve for a Slab on a Soil with $E_{soil} = 10kN/cm^2$. 103

7.27 Load - Central Deflection Curve for a Slab on a Soil with E_{soil} = $2kN/cm^2$. 104

7.28 Load - Central Deflection Curve for a Slab on a Soil with E_{soil} = $0.2kN/cm^2$. 105

7.29 Contours of the Equivalent Subgrade Modulus for a Soil with E_{soil} = $2kN/cm^2$ at Four Different Loads. 107

7.30 Contours of the Equivalent Subgrade Modulus for a Soil with E_{soil} = $10kN/cm^2$ at Four Different Loads. 108

List of Tables

7.1 Ultimate Loads for Four Cavities and without Cavity Considered for the Size Effect Study. 72

7.2 Ultimate Loads for Cavities I. II. & III for $k = 0.01kN/cm^3$ and $k = 0.1kN/cm^3$ 76

7.3 Ultimate Loads for Weak. Intermediate and Stiffer Soils for $\rho = 0.22\%$ and 0.32% 102

7.4 Load corresponding to 1" settlement for Weak. Intermediate and Stiffer Soils for $\rho = 0.22\%$ and 0.32% 106

Abstract

Name: Mansoor Ali Beg

Title: Numerical Modeling of RC Slabs on Tensionless Elastic Subgrade

Major Field: Civil Engineering

Date of Degree: July 1996

The problem of slabs resting on elastic soil is tackled by means of developing two nonlinear finite element programs, WINKLER and PSEUDO-3D. The program WINKLER is based on the classical Winkler hypothesis whereas a three dimensional elastic analysis is used in PSEUDO-3D. A tensionless behavior is considered for the subgrade, by assuming that the subgrade reacts only in compression. The existence of sinkholes/cavities underneath the slab is also modeled. The size effect and the location effect of such sinkholes on the behavior of reinforced concrete slabs are studied. A new concept of variable subgrade modulus values for a subgrade is introduced in the PSEUDO-3D model. The new model Pseudo-3D is compared and contrasted with the classical Winkler hypothesis. Contours of subgrade modulus as well as dimensionless equivalent subgrade modulus. for slabs on weak, intermediate, and stiff soils are presented.

Master of Science Degree
King Fahd University of Petroleum and Minerals
Dhahran, Saudi Arabia
July, 1996

خلاصة الرساله

اسم الطالب : منصور علي بيج

عنوان الرساله: النمذجه الحسابيه للقواعد الخرسانيه المرتكزه على التربه

التخصص : الهندسه المدنيه

تاريخ الشهاده : يوليو ١٩٩٦

في هذه الرساله تتم دراسه القواعد الخرسانيه المرتكزه على تربه مرنه بواسطه برنامجين للحاسب الالي تم تطويرهما باستخدام طريقة العناصر المحدوده. و يعتمد البرنامج الأول على نموذج "وينكلر" المعروف ، بينما يعتمد الثاني على معاملة التربه كجسم كبير ثلاثي الأبعاد. كما تمت معالجة التربه على اساس انها لا تقوم بتوفير مقاومه للقاعده في حالة الشد.

و قد أحتوت نتائج الرساله علي دراسه لتاثير وجود فجوات في التربه الواقعه تحت القاعده، بما يشمل تاثير حجم و موقع هذه الفجوات المؤثره . كما تم أعطاء نتائج و تصورات جديده لأستخدام نموذج "ونكلر" و لكن عن طريق قيم متغيره للمعامل و ليس قيمه ثابته. و قد أوضحت تلك النتائج أهميه الطريقه المقترحه و أفضليتها على بقيه النماذج الحسابيه المستخدمه لحل المسائل المشابهه.

درجه الماجستير في العلوم

جامعة الملك فهد للبترول و المعادن

الظهران ، المملكه العربيه السعوديه

يوليو ١٩٩٦

Chapter 1

INTRODUCTION

1.1 General

All civil engineering structures are built on soil or rock foundation. In general, the live and dead loads acting on such structures are transmitted to the foundation through individual footings or foundation slabs. It is also known that all soils compress noticeably when loaded; and cause the supported structure to settle. Hence, footings are to be designed to prevent excessive settlement, to minimize differential settlement, and to provide adequate safety against sliding and overturning. To limit the settlements it is necessary to transmit the loads of the structure to a soil stratum of sufficient strength and to spread the load over a sufficiently large area of that stratum, to minimize the soil bearing pressure. On the otherside, the structural failure of footings may be a flexure failure, a diagonal-tension failure (punching shear

failure) or a shear-compression failure.

Structural slabs or pavements such as highway pavements, airport runways and warehouse floors, are often supported directly by the natural ground surface or by a prepared and compacted sub-base and subgrade. They are commonly used because of their durability, and their ability to overcome subgrade weakness and difficult climatic conditions. Mostly due to non-uniform loading of such slabs, stresses develop which result in the failure of the slab itself. Failure may also be caused by unequal settlement, overloading, and restrained shrinkage or thermal displacements. One additional important element which might contribute to the initiation of pavement deterioration is the existence of voids or loss of support under the slab. As a result, the primary difficulty in the analysis of slabs on elastic foundation lies in the accurate determination of contact pressures between the structure and the foundation, which is dependent on the subgrade model used in the analysis.

1.2 Slabs-on-Grade

Pavements, runways, warehouse floors... etc., which are supported either directly on natural ground or a prepared subgrade, can be categorized as Slabs-on-Grade. The slab-on-grade behavior can be predominantly nonlinear, mainly due to material nonlinearities in the slab or soil. Material nonlinearities in the slab exist at high load levels due to cracking of concrete in tension, yielding and crushing of concrete

in compression, yielding of steel reinforcement, and the nonlinear response of subgrade soil. Other sources of nonlinearities include loss of support due to removal of subgrade material, curling of slabs under thermal gradients and the resulting closing of joints, and partial loss of contact. Material nonlinearities in the soil or subgrade are not considered in this study.

In some regions of the world there is a possibility of development of cavities or sinkholes under the foundation or pavement, due to erosion by ground-water, excavation works for temporary repairs, or soil compaction resulting from vibrations. Generally, if the soil beneath the foundation is underlain by a soluble limestone there is a greater possibility of cavity formation. These cavities eliminate the soil support beneath a portion of the foundation. Hence, the possibility of sinkholes or cavities must be considered during the design process.

1.3 Numerical Methods for Slabs-on-Grade

In the past, some experimental research has been done on reinforced concrete slabs resting on elastic foundation. But recently there has been more emphasis on the use of computational modelling as a powerful tool for the verification of experimental results. The finite element method and the finite difference methods seem to be the most common procedures employed in this area of modelling. Before the era of finite element method, the finite difference method was perhaps the most widely

used numerical technique.

In recent years, the finite element method has been an undisputed favorite in numerical studies of the problem of a slab or plate resting on an elastic foundation. The method can accommodate single and multiwheel loads, finite size slabs and all three fundamental loading conditions, i.e., interior, edge and corner and can also take care of different types of boundary conditions. As a result, nonlinear finite element analysis can be used effectively in the analysis of slabs-on-grade problems. This method can also be used for approximate but acceptable solutions for complex problems.

1.4 Subgrade Models

In terms of simplicity, subgrade modelling ranges between the two limits of the three-dimensional elastic foundation model and the Winkler, or the dense liquid, model. The three dimensional elastic foundation model though realistic, is very expensive computationally. The requirement of maintaining the aspect ratio of the individual elements at a reasonable limit, makes this model prohibitively expensive. In addition, proper modeling of the interface between the slab and subgrade adds to the complexity of the analysis. In most cases, the concrete slab is not bonded to the subgrade and this effect is difficult to achieve in this model.

On the other hand the Winkler-model is conceptually simpler, and computa-

tionally more efficient. According to Winkler hypothesis, the contact pressure p at a point of the foundation is a constant k times the vertical displacement w of that point: where k is called the modulus of subgrade reaction. Such a property is demonstrated by a medium consisting of a heavy liquid or independent springs.

In reality, the behavior of the soil differs considerably from the Winkler hypothesis. According to Winkler, a load causes a settlement only at the point where it is applied, but in reality the foundation is a continuous body and a continuous settlement curve should result. Therefore, the most serious drawback of this model is that the subgrade pressure on the slab at a point depends only on the deformation of the base spring below that point but not on the deflection of the springs around it.

1.5 Problem Definition

In the present work, the linear and nonlinear response of slabs on elastic soil, which are loaded uniformly or using patch loads is analyzed. Loss of contact of such slabs due to patch loads and also due to the existence of cavities/sinkholes beneath the slab is also modeled. To achieve this task, an already existing nonlinear finite element model 'FATIMA' written in FORTRAN by Abbasi [1], for the analysis of reinforced concrete slabs, is modified numerically. Basically, two different subgrade models, named, WINKLER and PSEUDO-3D, are formulated and used in this study.

1.6 Objectives

The primary objectives of this thesis work are:

1. To formulate the Winkler model in a mathematical form consistent with the Finite Element Method.

2. To incorporate additions and modifications in the existing source code 'FATIMA' to model subgrade according to the Winkler hypothesis.

3. To model the soil as a three dimensional elastic medium and link this model to the Winkler model so as to study the effect of subgrade reaction on slabs.

4. To study the effect of both subgrade models on the capacity of RC footings in particular and slabs-on-grade in general.

5. To include lift-off or loss of contact due to loading as well as due to cavities beneath the slab, using the Winkler model.

6. To investigate the size and location effect of subgrade cavities on the capacity of reinforced concrete slabs-on-grade.

7. To investigate the effect of a three dimensional analysis on the overall behavior and contrast it with the Winkler approach.

Chapter 2

LITERATURE REVIEW

This chapter presents a brief review of past research in the area of finite element analysis of RC slabs and slabs-on-grade. Also, literature on slabs on elastic foundation and general modeling of elastic soil mass is briefly surveyed.

2.1 Reinforced Concrete Slabs

Reinforced concrete is a challenging material for the structural analyst because of its inherent inhomogenity and nonlinearities. Several finite element models for reinforced concrete slabs have been developed to predict the nonlinear behavior of reinforced concrete. More recently, nonlinear finite element analysis applications to RC structures have improved remarkably due to research and advances in computer technology. Nonlinear finite element analysis results may become very sensitive to

geometric idealizations such as boundary and continuity modeling, discretization, finite element formulation, material and failure modeling, numerical strategies and computational parameters.

It is known that when reinforced concrete slabs are subjected to concentrated loads the problem of punching shear arises. Fernando, et al. [2], investigated the symmetrical punching of reinforced concrete slabs based on nonlinear finite element modelling. The model was used to predict the behavior up to ultimate conditions of various slabs under punching loads and the nature of the mechanism through which punching failure occurs. Eight-noded and three-noded axisymmetric isoparametric elements were used for concrete and steel respectively.

Generally, the primary reasons of nonlinearity in reinforced concrete are its plastic behavior in compression and cracking in tension. In addition, the reinforcing steel introduces another dimension of nonlinearity with its plastic behavior and interaction effects. These include bond-slip, tension-stiffening, and dowel action. Hence, there rises a need for sophisticated material models representing the experimentally observed responses of concrete and steel. A new elasto-plastic cracking constitutive model for the analysis of reinforced concrete was developed by Channakeshava and Iyengar [3]. The model considers the nonlinearities due to tensile cracking, aggregate interlock, plasticity in compression, yielding of steel, bond-slip and tension stiffening.

Lewinski and Wojewodzki [4] developed an integrated finite element model for

the analysis of reinforced concrete slabs, in which ten different cracking patterns were assumed in the formulation. When compared to the layered method, as used by most of the researchers, their model allows for the nonlinear analysis using relatively low numerical effort. The model was implemented using a 20 degrees of freedom plane rectangular element having only corner nodes, with five degrees of freedom at each node.

Abbasi [1] developed a nonlinear finite element model for the prediction of the flexural and shear response of RC concrete slabs by modelling various forms of degradation in the material throughout the loading history. The nonlinearities considered in his work include yielding, cracking and crushing of concrete and also elasto-plastic yielding of steel reinforcement. He employed 8/9 noded quadrilateral elements derived from the degeneration of a three dimensional shell element, for which five degrees of freedom per node were considered. Each element was divided into a certain number of steel and concrete layers, in order to observe the progressive degradation throughout the thickness of the element.

Huria, et al. [5] developed a nonlinear finite element model for the analysis of a RC slab bridge. They used degenerated isoparametric shell elements to model the deck. Their model had an option on the type of the element to be used, i.e., four noded flat quadrilateral element, eight noded serendipity element or the nine noded parabolic lagrangian element. A layered approach was also employed, in which the steel bars were represented by a smeared layer of steel. The behavior of each concrete

or steel layer was represented at the gauss integration points with predefined biaxial and uniaxial stress-strain models, respectively.

Finally an eight-noded quadrilateral shell element, with six degrees of freedom per node was used by Marzouk and Chen [6] for the finite element analysis of high-strength concrete slabs. A 2×2 reduced gaussian integration rule was used over the plane of each element, while a nine-point Simpson integration rule was selected through the element thickness to account for severe material nonlinearities introduced by concrete cracking and crushing, and reinforcement yielding.

2.2 Slabs-on-Grade

In 1867, Winkler [7] introduced the concept of subgrade reaction into applied mechanics. The concept was expanded in subsequent years to include the computation of the stresses in such flexible foundations as footings or slabs resting on soil.Several researchers have attempted to develop empirical relationships for the determination of the subgrade modulus k to solve beams and plates on elastic foundation problems. Vlasov and Leont'ev [8] postulated a two-parameter model using a theoretical approach to represent the soil continuum. Their model eliminated the need to determine the value of k, but it introduced a new parameter γ, which represents the variation of the deformation of the soil, whose value must be estimated and no procedure was provided for computing its value. Using variational principles , the

model developed by Vlasov and Leont'ev [8] was refined by Vallabhan, et al. [9], and a numerical model using the finite difference method was introduced to solve a rectangular plate resting on a layered soil medium. Instead of the coefficient of subgrade reaction of the soil, k, the elastic material properties of the soil were used in the analysis. The basic parameters required for the analysis were computed from the geometry and material properties of the soil and the structure.

A new adaptation of an existing finite difference solution to the problem of a plate resting on an elastic foundation was introduced by Ioannides [10]. Square elements were used for discretizing the slab. The effect of slab size, for three loading conditions i.e., interior, edge and corner, was investigated. The limits for the development of infinite slab responses were established for each of the three loading cases. Comparing the results with closed-form solution and other numerous convergence studies, the effectiveness of finite difference method was compared to that of finite element method.

It should be noted that the response of elastic plates resting on a Winkler foundation has been studied by many investigators by assuming that the foundation reacts in tension as well as in compression . However, the solution method required to determine the realistic response of plates supported by tensionless foundation is more complicated, because the contact region is not known in advance. Therefore, the solution of tensionless foundation problems requires an iterative approach to deal with the non-linear system of equations, even for elastic linear behavior.

Villaggio [11] studied the contact region of a plate on an elastic foundation that reacts only in compression, when loaded with a central concentrated load, by employing the boundary element method. In his approach, he assumed an elliptic contact region for the case of a rectangular plate. Also, the behavior of elastic plates of rectangular shape on a tensionless Winkler foundation has been investigated by Celep [12], by considering distributed and concentrated loads without any assumption on the shape of the contact region. Khathlan and Waly [13] investigated the unbonded contact problem for an annular elastic circular plate resting on a tensionless Winkler elastic foundation by employing the concept of minimizing the total potential energy of the plate-foundation system. The common factor between these three independent studies [11, 12, 13] is the use of the Winkler model and the emphasis given to the determination of the size of the contact zone. The three studies have all proven that the size of the contact zone is independent of the value of the load.

Meyerhof and Rao [14] conducted a series of studies on the load-carrying capacity of floating ice-sheets, concrete pavements, and footings by using the theory of plasticity. They obtained interesting results on spread footings by considering the contact pressure with the subgrade soil under the footing. Using the theory of plasticity, the collapse load of a reinforced concrete square spread footing under column load was also studied by Jiang [15]. The influence of nonuniform soil pressure under the footing slab upon its carrying capacity was also investigated. A

comparison between the theoretical results and existing test data indicates that the average measured collapse load is higher than the least upper bound; which may partly be attributed to the change in the contact pressure, especially near failure. If the subgrade reaction is not uniformly distributed, the collapse load of the footing will obviously be different.

A study on the concentrated load carrying capacity of concrete slabs on ground was carried out by Rao and Shashikant [16], using lower-bound limit analysis solutions. A rigid plastic behavior and square yield criterion of failure was assumed. Concentrated loads at the interior, near the edge, at the edge, and at the corner were considered in their study.

Using the finite element method, Chou [17] analyzed stress conditions in small concrete precast square slabs-on-grade connected at the joints by load-transfer devices. The natural subgrade soil is simulated by a series of springs, i.e., a Winkler model. It was noted that when the size of a small concrete slab is increased, the stresses are increased for any loading position and the change becomes insignificant when the slab size has increased beyond a certain value. Another study by the same author [18] investigates the subgrade contact pressure under rigid pavements, using the finite element method for concrete slabs on elastic subgrade. A concrete pavement is analyzed by the Westergaard solution on a dense liquid subgrade with a subgrade modulus k, and by the finite element method on an elastic subgrade with modulus of elasticity E_s, and it is concluded that no unique relation exists between

E_s and k. Losberg [19] developed solutions of airport pavements using the equilibrium method of yield line theory. A similar problem was solved using the virtual work method by Baumann and Weisgerber [20] with the soil behavior represented by a Winkler model.

A finite element model for slab-on-grade problem was introduced by Nasra and Wang [21], where the concrete slab is represented by 8-node brick elements, and the expansion joints and the subgrade are represented by boundary-spring elements. The subgrade elements are taken to be non-tension elements to represent the soil resistance characteristics. In addition, the effects of temperature and moisture gradients, slab thickness, modulus of subgrade reaction and modulus of elasticity of concrete are also studied. The study of the response of a warped slab to point loads concluded that the contact area increases as the applied point load increases. Also, the increase in the contact area from the subgrade improves the supporting reaction and thus, improves the performance of the slab. For the case of corner loadings, as well as edge loadings, it was shown that lower subgrade moduli result in higher cracking loads. The reason is that since the subgrade modulus is low, the slab will sink deeper and thus obtain more support, and hence resistance to external loads.

Nogami and Lam [22] analyzed slabs on elastic foundation using a two-parameter model in which the foundation medium is divided into a number of horizontal layers. Each layer is idealized by a system of one-dimensional vertical columns interconnected by shear springs.

Ioannides and Donnelly [23] investigated the response of flexible and rigid pavements on stress-dependent foundation, using a three-dimensional finite element program. The effects considered in the analysis were mesh fineness, vertical and lateral subgrade extent, and boundary conditions for both the interior and edge loading conditions. They concluded that subgrade stress dependence may be important primarily when considering heavy edge and corner loads: and also that it affects the maximum subgrade stress to a much greater extent than the maximum deflection or bending stress.

Sakurai, et al. [24] used an integral equation method for the three dimensional analysis of footings resting on a semi-infinite elasto-plastic medium. A square foundation resting on a semi-infinite elastic-perfectly plastic medium is considered in their study. For a case of rigid foundation, the resultant forces of contact pressure at different settlement levels did not show much difference in comparison to that of elastic analysis. Therefore, as far as the resultant forces are considered an elastic analysis is sufficient. Similarly for a flexible foundation, comparison of displacement by both elastic and elasto-plastic analysis resulted in an insignificant difference.

Channakeshawa et al. [25] studied dowel-jointed concrete pavements, by using non-linear finite element analysis. The non-linearities considered are cracking of concrete in tension, compressive yielding of concrete, and loss of support due to lift-off of pavements because of thermal gradients. Analysis of plain concrete pavements subjected to self-weight, temperature gradients and static wheel loads were

performed with four different extents of loss of subgrade support and two different dowel-concrete interface characteristics.

Design charts based on a finite element analysis are presented for a rigid pavement slabs of finite size for both central and edge loading conditions, by Sargious and Wang [26]. The main variables considered are the thickness of the slab, the modulus of elasticity of the subgrade and the values of the load and tire pressure. The authors treated the subgrade as an elastic continuum in the analysis, where the stiffness of each subgrade element is represented by a stiffness matrix rather than by one constant stiffness coefficient, as in the case with Winkler-type foundation. The charts are useful in determining thickness of a highway or airfield rigid pavement required to carry a certain central or edge wheel load and also useful in checking maximum stress in an existing pavement.

Finally, a study was made by Richart and Zia [27] for beams and slabs that span sinkholes or cavities in the elastic subgrade, by making use of the theory of elastic subgrade reaction. Their work delineates the effect of loss of support on foundation design; and also provides design curves. The effect of local loss of support on the stresses and deformations developed in the foundation structures is also presented. For a slab spanning a cavity, comparison of the moments and deflections resulting from uniform loads with those resulting from a concentrated load showed that the dead weight of the slab produced approximately one-third of the total deflection.

Chapter 3

NON-LINEAR FINITE ELEMENT MODELING OF RC SLABS

In this chapter an overall view of the non-linear finite element model for the analysis of reinforced concrete slabs is presented. The formulation follows the model developed and described in detail by Abbasi [1]. The following sections give a brief description of the main features of that model, highlighting the ones relevant to this study.

3.1 Material Modeling

One of the important and challenging tasks in modeling of concrete is to model the complex material behavior which includes the non-linear behavior, tensile cracking, biaxial yielding, strain softening phenomenon, modeling of post fracture behavior and interaction effect between the concrete and the reinforcing bars.

3.1.1 Behavior of Concrete

In order to simulate the material behavior and to determine the various material constants in the mathematical model, concrete under uniaxial and biaxial states of stress is studied.

Generally, for normal strength concrete, the linear elastic behavior extends to about 30% of its maximum compressive strength, f'_c. The uniaxial compressive stress-strain curve shown in Figure 3.1 is employed for modeling of strain hardening behavior of multiaxial state of stress. The linear elastic behavior is assumed up to stress equal to $0.3f'_c$ and beyond this level a parabolic stress-strain relationship is assumed with strain corresponding to peak stress equal to $(2f'_c)/(E_o)$ for normal concrete, where E_o is the initial modulus of elasticity. Beyond this peak, the stress is assumed to be constant at increasing strain until crushing failure occurs at the ultimate strain, ϵ_u.

The stress-strain curve in tension is assumed to be linearly elastic up to maximum

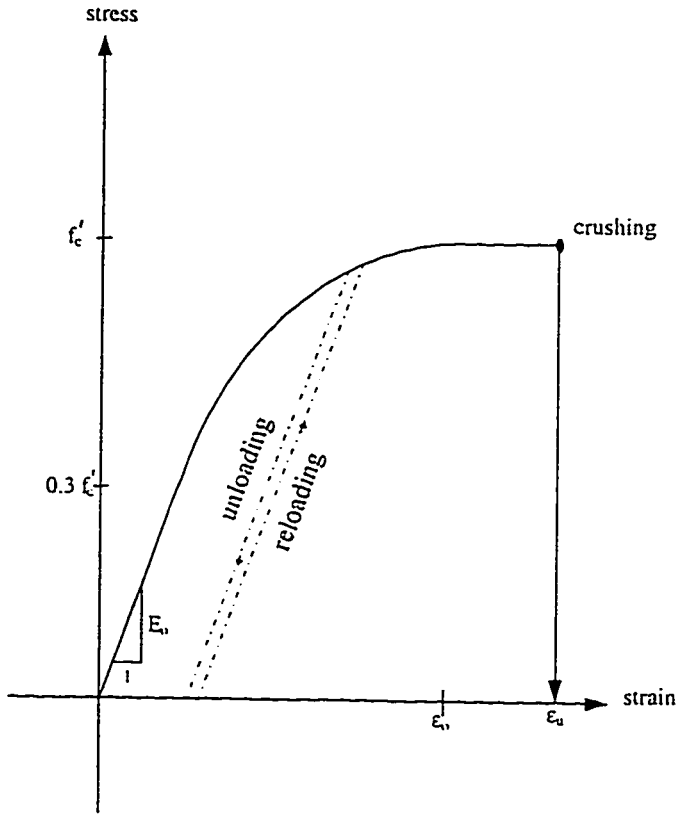

Figure 3.1: Uniaxial Compressive Stress-Strain Curve for Concrete.

tensile strength f'_t. The tensile strength f'_t, being calculated either by split-cylinder tensile strength $6\sqrt{f'_c}$ or by the modulus of rupture $7.5\sqrt{f'_c}$.

For modeling of compressive failure in the concrete, a multiaxial constitutive relationship is essential. To achieve that several different yield criteria exist, such as Von Mises, Tresca, Mohr-Coulomb, Drucker Prager and a new model proposed by Abbasi [1]. In this numerical study the Mohr-Coulomb yield criterion is being employed for the analysis.

The Mohr-Coulomb yield criterion can be mathematically described using

$$\tau = c - \sigma(tan\phi) \tag{3.1}$$

where τ and σ are shear and normal stresses on any plane at a point in a concrete material, and ϕ is the angle of internal friction for concrete and is taken as 37^o [28]. The material constant c is given in terms of f'_c and ϕ as follows:

$$c = \frac{f'_c(1 - sin\phi)}{2cos\phi} \tag{3.2}$$

In terms of principal stresses (σ_1 and σ_3), Equation 3.1 can be written as

$$\frac{\sigma_1(1 + sin\phi)}{2c(cos\phi)} - \frac{\sigma_3(1 - sin\phi)}{2c(cos\phi)} = 1 \tag{3.3}$$

In addition, the crushing of concrete is based on a strain-controlled phenomenon. A specific point in concrete is assumed to lose all its characteristics of strength once

it reaches the ultimate total strain ϵ_u, which is taken as 0.0035.

For concrete in tension, in the vicinity of a crack in the concrete, the load is assumed to be totally carried by the reinforcement and between cracks the load will be shared by both concrete and reinforcing steel. This tensile behavior of reinforced concrete can best be modeled using a tension-stiffening model, schematically described in Figure 3.2. In this mode, concrete is assumed to behave linearly upto the tensile strength f_t, which defines the initiation of a crack. Further increase in strain cause a sudden drop in the stress followed by a gradual reduction to zero at the maximum strain value ϵ_m.

3.1.2 Behavior of Steel

A bilinear stress-strain behavior is considered for steel. The steel bars in the concrete are represented in the model by a smeared layer of steel extending upto the total length and width of the slab. The thickness of this layer can be evaluated from the total amount of steel reinforcement bars. Steel in two orthogonal directions is represented by two layers of steel in opposite directions which bend only in one direction.

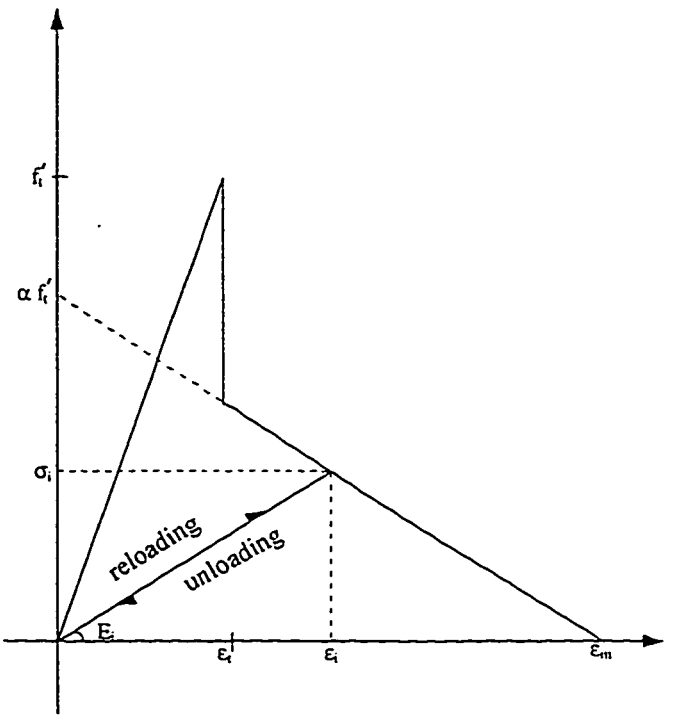

Figure 3.2: Tension-stiffening Behavior in Cracked Concrete.

3.2 Finite Element Model

In the non-linear finite element code 'FATIMA' developed by Abbasi [1], eight/nine noded quadrilateral elements derived from a three dimensional shell element were used. The degrees of freedom considered at each node are three displacements and two rotations.

3.2.1 Element Description

In this study, the nine-noded Lagrangian degenarated thick shell element is employed. The nodal configuration for the nine-noded lagrangian element is shown in Figure 3.3. The shape functions for this element are as follows [1]:

For corner nodes $i = 1,3,5,7$

$$N_i = \frac{(\xi^2 + \xi\xi_1)(\eta^2 + \eta\eta_1)}{4} \tag{3.4}$$

For mid-side nodes $i = 2,4,6,8$

$$N_i = \frac{\eta_i^2(\eta^2 - \eta\eta_i)(1 - \eta^2)}{2} + \frac{\xi_i^2(\xi^2 - \xi\xi_i)(1 - \xi^2)}{2} \tag{3.5}$$

and for the central node ($i = 9$) the bubble shape function is given by

$$N_i = (1 - \xi^2)(1 - \eta^2) \tag{3.6}$$

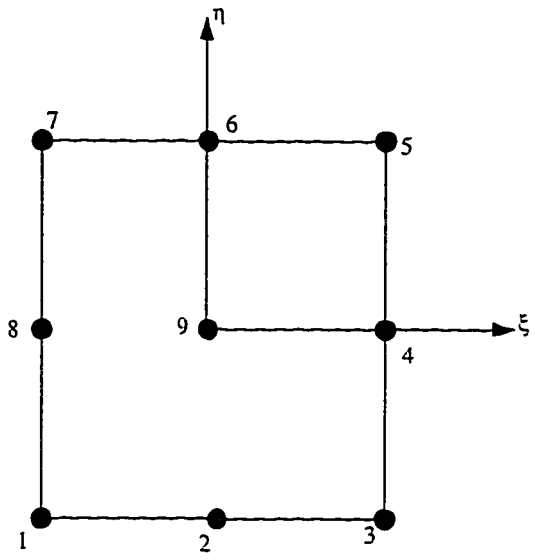

Figure 3.3: Nodal Configuration of 9-noded Lagrangian Element.

3.2.2 Slab Element Stiffness Matrix

The element stiffness matrix is given as

$$[K] = \int_V [B]^T [D][B] dV \tag{3.7}$$

where [B] is a matrix relating the strain vector $\{\epsilon\}$ to the displacement vector $\{d\}$ as follows

$$\{\epsilon\} = [B]\{d\} \tag{3.8}$$

and [D] is a matrix of the elasto-plastic material stress-strain relation.

In normal coordinates Equation 3.7 results in the 45 × 45 slab element stiffness matrix.

$$[K] = \int_{-1}^{+1} \int_{-1}^{-1} \int_{-1}^{+1} [B]^T [D][B] \, |J| \, d\xi d\eta d\zeta \tag{3.9}$$

3.2.3 Numerical Integration

Efficiency and accuracy of the isoparametric plate bending element depends on the numerical integration employed. In the thickness direction, the integration is simplified with the use of a layered model. A selective integration scheme is employed for integrating at any layer mid-surface. For bending and membrane terms a normal integration rule is employed, i.e., 3×3 rule: and for shear terms a 2×2 integration rule

is employed. The selective integration scheme eliminates the locking phenomenon, which may be faced when a full integration rule is used.

3.2.4 Layered Approach

One of the interesting features of the adopted non-linear model is the layered approach employed through the thickness of each element. This is an advantageous aspect for modeling of plates where there exists more than one material in an element, e.g. reinforced concrete. The total thickness of an element is divided into a certain number of layers of concrete and steel, Figure 3.4. In this case, the steel bars are modeled using a smearing approach. Layers are numbered sequentially, starting at the bottom surface of plate. Each layer contains its own Gauss integration points on its mid-surface.

3.2.5 Finite Element Solution

An iterative and incremental approach is the backbone of the non-linear finite element analysis. The element stiffness matrix can be determined once [B] and [D] matrices are evaluated. Matrix [B] is evaluated at each Gauss integration point of each layer of all elements only at the beginning. The elasto-plastic matrix [D] may need to be updated during each iteration depending on the material status of concrete and steel. The slab stiffness matrix $[K]$ is calculated by performing numerical integration within the layers and summation through the thickness over all layers.

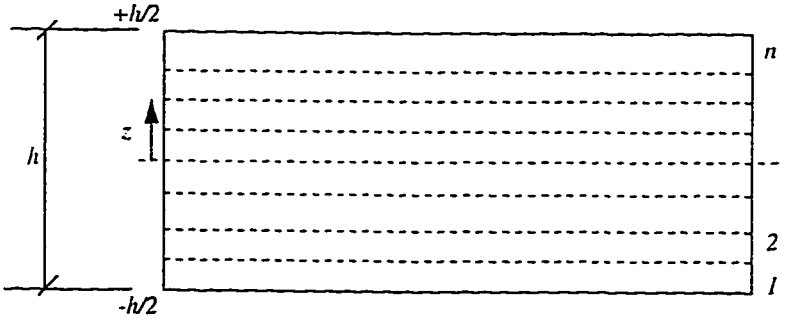

Figure 3.4: Layered Element Model for Reinforced Concrete Slab.

Then the frontal solver is used for solving the equations of equilibrium using the calculated element nodal loads. The equations of equilibrium are assembled, and the variables are eliminated at the same time. The most obvious advantage of this technique is that it solves the equations by handling each element stiffness one at a time. To start the analysis, the material status for steel and concrete Gauss points is initialized as elastic. The elements are loaded in an incremental fashion.

For an r^{th} load increment and an i^{th} iteration the process that takes place for an incremental and iterative approach is as follows:

For an r^{th} load increment, the displacements $\{d\}^{r-1}$, the stresses $\{\sigma\}^{r-1}$ and the unbalanced nodal forces $\{\psi\}^{r-1}$ of previous load increment are known.

For an r^{th} load increment of $\{df\}^r$ the incremental nodal forces are given by

$$\{\psi\}^r = \{\psi\}^{r-1} + \{df\}^r \tag{3.10}$$

For a generic iteration, i, the iterative process consists of the following steps:

1. The stiffness matrix [K] is recalculated in the first or second iteration of every load increment.

2. The incremental displacements $\{\Delta d\}^i$ are calculated by

$$\{\Delta d\}^i = [K]^{-1}\{\psi\}^{i-1} \tag{3.11}$$

where $\{\psi\}^{i-1}$ are the unbalanced nodal forces resulting from the previous iteration.

3. Then the total displacement vector $\{d\}^i$ is updated,

$$\{d\}^i = \{d\}^{i-1} + \{\Delta d\}^i \tag{3.12}$$

4. The incremental strains $\{d\epsilon\}^i$ and the total strains $\{\epsilon\}^i$ are evaluated using,

$$\{d\epsilon\}^i = [B]\{\Delta d\}^i \tag{3.13}$$

$$\{\epsilon\}^i = [B]\{d\}^i \tag{3.14}$$

where [B] is the strain-displacement relation matrix at a Gauss point.

5. The incremental stresses $\{d\sigma\}^i$ and the total stresses $\{\sigma\}^i$ are then calculated using,

$$\{d\sigma\}^i = [D]\{d\epsilon\}^i \tag{3.15}$$

$$\{\sigma\}^i = \{\sigma\}^{i-1} + \{d\sigma\}^i \tag{3.16}$$

where [D] is the revised elasto-plastic matrix which reflects any changes due to material degradation.

6. Using the material constitutive equations, the stresses are then corrected .

7. The equivalent internal nodal forces $\{p\}^i$ are evaluated using the following numerical integration

$$\{p\}^i = \int_V [B]^T \{\sigma\}^i dV \tag{3.17}$$

8. The residual or out-of-balance forces, $\{\psi\}^i$ are then calculated as

$$\{\psi\}^i = \{f\}^i - \{p\}^i \tag{3.18}$$

where $\{f\}^i$ is the current external nodal force vector.

Finally, the convergence of the solution is checked according to a certain prescribed criterion. If convergence is achieved, then the next load increment is taken into account and the same iterative steps are repeated. Otherwise, the analysis is continued by starting a new iteration within the same increment until the solution converges.

Chapter 4

WINKLER SUBGRADE MODELING

In this chapter the fundamentals of modeling of the subgrade by Winkler hypothesis are presented. The loss of contact situations due to lift-off of corners of the slab or due to sinkholes are explained. and also the methodology adopted is also described in detail.

4.1 Description

The problem of a plate on a soil mass or a footing transmitting load to a soil stratum is very complicated, because of the nature of reaction of the subgrade or soil underneath the plate or footing. One of the earliest works in tackling such

subgrade problems was done by Winkler in 1867 [7]. According to his hypothesis the contact pressure p at a point is directly given by the product of a constant k and the displacement w at that point. Mathematically,

$$p = kw \tag{4.1}$$

where k is called the modulus of subgrade reaction.

Till this date, in most of the analysis of footings or slabs resting on soil, this hypothesis is being used, mainly because of its simplicity. The main drawback of this hypothesis is that the subgrade pressure at one point is not at all effected by displacement at any other point, which is not the case in reality. Moreover, a uniform value of subgrade modulus has to be used to carry-out the analysis, and is usually difficult to define for a specific soil. For example, when a plate is loaded with uniformly distributed load, then Winkler hypothesis gives a rigid-body settlement profile instead of a dishing profile, which reflects its inaccuracy.

A lot of research has been devoted in determining the right value of modulus of subgrade reaction k. An estimate of a value of k depends on the type of soil, depth of strata, modular ratio of the structure and the soil, and more importantly the distribution of the loading on the slab. As a result, this difficulty of evaluating k has shown that the use of the Winkler model can lead to a non-conservative design values, for certain load situations.

4.2 Loss of Contact Problem

The response of a slab on an elastic foundation is usually determined by assuming that the contact between the foundation and the slab is provided continuously, whether the foundation reaction is compression or tension. The slab may have a partial contact with the foundation if the edges of the slab are not anchored against lift-off, which is the usual case. For partial contact situations, the applied forces will be carried out only within the contact area. In most cases, the contact zone of the slab with the soil is not known in advance as it depends on the relative stiffness of the slab and the elastic foundation and the applied load. As a result, the loss of contact problem introduces a non-linear system of equations even for elastic loads. Hence, the solution of such problems inevitably involves the use of an iterative algorithm.

Another type of loss of contact exists due to sinkholes or surface cavities underneath the slab or footing. Their effect on the slab capacity is much more serious compared to the corner lift-off cases. The location and the size of the cavity makes the problem of slab on the subgrade more critical and it greatly changes the capacity of the slab or footing.

4.3 Methodology for Modeling

The methodology adopted for incorporating the Winkler model involves some changes and additions in the solution algorithm for the reinforced concrete slab element as

given in Section 3.2.5. The methodology is explained in the following steps:

1. A constant value of modulus of subgrade reaction k is used throughout the domain of the slab.

2. At the start of the analysis, the slab is assumed to be in full contact with the soil.

3. The element subgrade stiffness matrix $[S]$ is calculated using the constant value of k.

4. The plate element stiffness matrix $[K]$ is updated by adding the contributions from the subgrade stiffness $[S]$ to obtain the total stiffness matrix for the elements.

5. The equivalent nodal forces vector $\{p\}_{soil}$ as generated by the soil reaction is then calculated.

6. The plate equivalent nodal forces vector $\{p\}_{slab}$ is updated using the contributions of the subgrade reactions as given by $\{p\}_{soil}$.

Then the analysis is carried-out in a similar fashion as described in Section 3.2.5, till the convergence criteria is satisfied.

In step 2, the contact of the slab with the soil is assumed to be full; but the model has to take into account the problem of loss of contact due to both the lift-off condition and also the sinkhole case. The model is designed in such a way

that the analysis of the slab on subgrade can be carried-out with and without the phenomenon of loss of contact to be taken into account at the beginning. Modeling the loss of contact phenomenon involves some modifications to both the subgrade stiffness matrix $[S]$ and the subgrade nodal forces $\{p\}_{soil}$. These modifications can be itemized as follows:

- The displacement of a Gauss point of the slab is checked first.
- If the point is displaced above the initial level of the subgrade then it has lost contact with the soil. Therefore, the contribution of that point is not taken into consideration for both the subgrade stiffness matrix $[S]$ and for the subgrade nodal forces $\{p\}_{soil}$.
- If the point is displaced downward then the point is still in contact with the subgrade and it contributes in the evaluation of subgrade stiffness matrix $[S]$, and subgrade nodal forces $\{p\}_{soil}$. Then the next point is checked for the loss of contact.

4.4 Finite Element Formulation

The stiffness matrix of the slab element, $[K]$ as given by Equation 3.7 needs to be modified to include the effect of the subgrade reaction. The total potential energy of an elastic foundation is given by

$$U_{e.f.} = \frac{1}{2}\int kw^2 dA \tag{4.2}$$

where the vertical displacement of the slab is given by $w = [N]\{d\}$.

Here $\{d\}$ is the displacement vector containing only the nine vertical displacement components, w of the Lagrangian element. Consequently, the subgrade stiffness matrix $[S]$ can be given as

$$[S] = \int_A k[N]^T[N]dA \tag{4.3}$$

In terms of natural coordinates Equation 4.3 becomes

$$[S] = \int_{-1}^{+1}\int_{-1}^{+1} k[N]^T[N]\,|J|\,d\xi d\eta \tag{4.4}$$

This results in a 9 × 9 matrix containing the subgrade stiffness effect on the vertical displacements of all the nine nodes. The stiffness matrix as formulated by Equation 4.4 needs to be transferred to the slab stiffness matrix given by Equation 3.9. The contribution of the subgrade stiffness $[S]$ will only effect the vertical displacement components of the slab stiffness $[K]$.

The equivalent nodal forces for the slab element as given by Equation 3.17 also need to be modified to account for the vertical support of the slab by the soil. The contribution as given by the elastic foundation is added to the equivalent nodal forces as follows:

1. From Equation 3.17, the equivalent nodal forces due to internal stresses in the slab are given as

$$\{p_{slab}\} = \int_V [B]^T \{\sigma\} dV \tag{4.5}$$

2. In natural coordinates, Equation 4.5 is given by

$$\{p_{slab}\} = \int_{-1}^{+1} \int_{-1}^{+1} \int_{-1}^{+1} [B]^T \{\sigma\} |J| \, d\xi d\eta d\zeta \tag{4.6}$$

3. In addition, the contribution of the elastic foundation is given by

$$\{p_{soil}\} = [S]\{d\} \tag{4.7}$$

where $\{d\}$ is a 9×1 matrix containing only the nine vertical displacements. The updated equivalent nodal forces are given by

$$\{p_{total}\} = \{p_{slab}\} + \{p_{soil}\} \tag{4.8}$$

Following this formulation, the original slab element stiffness matrix and nodal force vector would be replaced by their new counterparts which include the contribution of the Winkler subgrade. However, in situations that involve no subgrade, the subgrade contributions obviously vanish, leaving the slab formulations unaffected.

Chapter 5

PSUEDO-3D SUBGRADE MODEL

This chapter explains the modeling of subgrade using the three dimensional analysis. The relation between the Winkler model and the three dimensional model is given in detail.

5.1 Description

The realistic behavior of a slab or footing on a soil mass can be ascertained only when the right value of subgrade modulus, k , is used. Using a specific, uniform coefficient of subgrade reaction will allow for an approximate analysis of foundation. However, the use of a uniform modulus of subgrade reaction is not consistent with the actual

behavior of soils. Therefore, zones of variable subgrade moduli are considered, to provide a more accurate estimate of the subgrade response as compared to that predicted by a single modulus of subgrade reaction. But there exists a difficulty in determining these zones and the variable subgrade moduli.

In the proposed PSEUDO-3D model the problem of a slab on a soil mass is carried-out by modeling the soil as a three dimensional elastic solid and then representing it as a Winkler model. The advantages of this model include the determination of the variable value of modulus of subgrade reaction which is a more advanced version of the Winkler model. The variable value of k eliminates the main drawback of the Winkler model of assuming a constant k throughout the analysis, and partially satisfies the slab-soil continuity condition.

5.2 Methodology of Modeling

The realistic behavior of a slab resting on a soil can be studied by employing a full three dimensional analysis of the soil and linking it to the slab. The computing cost for such a model will be enormously high. Such a model involves the development of an interface element between the slab and the soil. Moreover, modeling the loss of contact for such a model makes the computing cost enormously high. Hence a sophisticated method has to be employed for linking the slab to the soil. Using the Winkler model, as well as the advantages of the three dimensional model, the

PSEUDO-3D model, represents a sophisticated model for predicting the behavior of a slab on an elastic soil. The methodology for the PSEUDO-3D model is as under:

1. An arbitrary initial value of modulus of subgrade reaction k is taken as an input and is assumed to be applicable for whole slab domain.

2. At the start of the analysis the slab is assumed to be in full contact with the soil.

3. The subgrade stiffness $[S]$ is calculated using the assumed uniform value of k.

4. The plate stiffness $[K]$ is updated by adding the contributions from the subgrade stiffness $[S]$. following the same procedure of the Winkler model (Section 4.3).

5. The equivalent nodal forces $\{p\}_{soil}$ as generated by the soil reaction are then calculated, following the same procedure of the Winkler model (Section 4.3).

6. The nodal forces vector $\{p\}_{soil}$ is supplied to the three dimensional model as a load vector.

7. The stiffness matrix $[S]_{3d}$ for each element of the three dimensional soil body is calculated.

8. The vertical stresses of the top layer of the soil mass are calculated.

9. Then the new variable subgrade modulus, referred to as equivalent subgrade modulus, is calculated using the displacement at a point of soil mass and the stress given at that point. (Mathematically k at a point i is given by $k_i = \sigma_i / w_i$).

10. The equivalent subgrade modulus k_i is used in calculating the $\{p\}$ vector as given by Equation 4.8.

11. Then the convergence criteria is checked.

Since an iterative and incremental approach is employed in this analysis, the equivalent subgrade modulus is calculated for each Gauss point depending on the stress and displacement of the point in the soil mass. Thus the different subgrade modulus values at different points give a more realistic picture of the problem of slab-on-grade.

The modeling of loss of contact behavior for the PSEUDO-3D model differs from that of WINKLER. In WINKLER model, the Gauss point displacement in the slab was used as the criterion, whereas in PSEUDO-3D the stress level of the soil is used in evaluating the loss of contact behavior. If at a point in the top layer of the three dimensional soil body the vertical stress becomes tensile then it is assumed that the slab at that point loses contact with the soil. On the other hand, if the vertical stress is compressive then that point is considered in full contact with the soil.

5.3 Three Dimensional Element

A three dimensional hexahedral element with 27 nodes, as shown in Figure 5.1, is employed for the analysis of the soil mass. Three degrees of freedom corresponding to the translations in the x, y, and z directions, are considered at each node. Thus, the total number of degrees of freedom for this element is 81. The shape functions employed are the quadratic Lagrangian functions used for the plate element (Equations 3.4, 3.5, 3.6) but extended in three dimensions.

5.4 Finite Element Formulation

The element coordinates system (x-y-z) is related to the element nodal cartesian coordinates as follows:

$$x = \sum N_i x_i \tag{5.1}$$

$$y = \sum N_i y_i \tag{5.2}$$

$$z = \sum N_i z_i \tag{5.3}$$

The above three equations can be represented as:

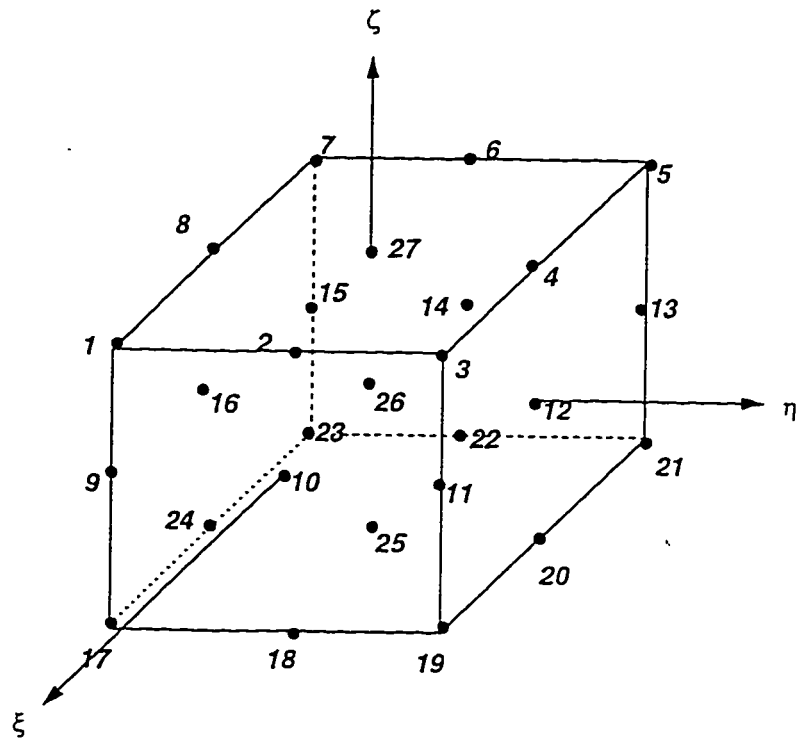

Figure 5.1: Nodal Configuration of Three Dimensional Hexahedral Element.

$$\left\{ \begin{array}{c} x \\ y \\ z \end{array} \right\}_{3\times 1} = [N]_{3\times 81}\{X\}_{81\times 1} \tag{5.4}$$

Similarly, the three translations at any point can be represented as:

$$\{u\}_{3\times 1} = [N]_{3\times 81}\{d\}_{81\times 1} \tag{5.5}$$

The strains are related to displacements as:

$$\{\epsilon\} = [B]\{d\} \tag{5.6}$$

where

$$\{\epsilon\} = \left\{ \begin{array}{c} \epsilon_x \\ \epsilon_y \\ \epsilon_z \\ \gamma_{xy} \\ \gamma_{yz} \\ \gamma_{zx} \end{array} \right\} = \left\{ \begin{array}{c} \frac{\partial u}{\partial x} \\ \frac{\partial v}{\partial y} \\ \frac{\partial w}{\partial z} \\ \frac{\partial u}{\partial y} + \frac{\partial v}{\partial x} \\ \frac{\partial v}{\partial z} + \frac{\partial w}{\partial y} \\ \frac{\partial w}{\partial x} + \frac{\partial u}{\partial z} \end{array} \right\} \tag{5.7}$$

and the stresses are related to strains as

$$\{\sigma\} = [D]\{\epsilon\} \tag{5.8}$$

where [D] is the three dimensional elasticity matrix and given as follows:

$$[D] = \frac{E}{(1+\nu)(1-2\nu)} \begin{bmatrix} (1-\nu) & \nu & \nu & 0 & 0 & 0 \\ \nu & (1-\nu) & \nu & 0 & 0 & 0 \\ \nu & \nu & (1-\nu) & 0 & 0 & 0 \\ 0 & 0 & 0 & \frac{1-2\nu}{2} & 0 & 0 \\ 0 & 0 & 0 & 0 & \frac{1-2\nu}{2} & 0 \\ 0 & 0 & 0 & 0 & 0 & \frac{1-2\nu}{2} \end{bmatrix} \tag{5.9}$$

The three dimensional element stiffness matrix $[S]_{3d}$ is given by

$$[S]_{3d} = \int_V [B]^T [D][B] dx dy dz \tag{5.10}$$

In terms of natural coordinates Equation 5.10 is given by

$$[S]_{3d} = \int_{-1}^{+1} \int_{-1}^{+1} \int_{-1}^{+1} [B]^T [D][B] |J| \, d\xi d\eta d\zeta \tag{5.11}$$

Using this formulation, the equivalent nodal forces as given by Equation 4.7 are applied to the three dimensional soil element. Stresses as given by Equation 5.8 are used in calculating the equivalent subgrade modulus. For a specific surface Gauss point, the calculation of the variable subgrade modulus is given by:

$$k_i = \sigma_i / w_i \tag{5.12}$$

where σ_i and w_i represents the vertical stress and vertical displacement of that point respectively.

Chapter 6

NUMERICAL ASPECTS AND PROGRAM DESCRIPTION

In this chapter, the programming aspects of the two models (WINKLER and PSUEDO3D) are explained. Flowcharts, description of subroutines and other features of both numerical models are described in detail.

6.1 Introduction

The two separate programs WINKLER and PSEUDO3D are written in FORTRAN code, using the same format adopted by Hinton & Owen [29, 30] for their reinforced concrete simply supported slabs. These are written in a modular form consisting of many subroutines called from the main program and also from within other

subroutines. Suitable outputs are generated for plotting the load versus deflection curves as well as many other useful parameters. Optional output is also provided to monitor the displacement, stresses and the reactions for any iteration and any increment. The material status of concrete and steel is also monitored and is updated continuously. In addition, the loads that cause the initiation of the yielding of concrete, one way cracking, two way cracking, crushing of concrete, yielding of steel, and the ultimate loads are all outputed so as to have a clear view of the slab degradation throughout its loading history.

6.2 Program WINKLER

This section describes the main programming features of the program WINKLER, based on the theoretical formulation given in chapter 4.

6.2.1 Material and Finite Element Parameters

The material parameters used to define the concrete material in the model includes, the Mohr-Coulomb yield criterion for concrete defined by the data variable NCRIT, strain hardening of the concrete defined by NHARD. For the concrete material, the tension-stiffening parameters of concrete are given by ϵ_m and α. Young's modulus of concrete by E_c, the concrete Poisson's ratio by ν which is taken equal to zero for all the numerical examples. The angle of internal friction ϕ, concrete ultimate

tensile strength f'_t, concrete ultimate compressive strength f'_c, concrete ultimate compressive strain ϵ_u are also defined for the concrete material.

For the steel material a bilinear elasto-plastic behavior is assumed. The parameters used to define the material include Young's modulus of steel E_s, Elasto-plastic Young's modulus E_{ep}, and the steel yield stress given by f_y. In addition, the thickness of the smeared steel layer and its locations across the slab thickness, are also defined.

The finite element parameters used to define the model includes the element type, the type of solution algorithm used, and the integration scheme employed. A 9-noded Lagrangian element with five degrees of freedom per each node is used for the analysis of the slab. For computational economy reasons, the stiffness matrix $[K]$ of the slab is re-calculated only in the second iteration of each increment. A selective integration scheme (3×2) rule is employed. For the layered approach, each element is divided into eight concrete layers and two steel layers. Concentrated loads as well as uniformly distributed loads can be used in the analysis, and the boundary conditions for the slab elements are specified by the translations u, v, w, and rotations β_1 and β_2. For all the cases in this study, the slab boundaries are considered free, which restricts boundary conditions to the symmetry axes only as applicable. A displacement norm is used for the convergence criteria which is verified by a tolerance value within a specified maximum number of iterations. Displacements, reactions, stresses, stress resultants, and material status can be outputed at any iteration of any increment.

Also an optional output for plotting the load deflection curves is provided.

6.2.2 Main Data Variables

In this model, the modulus of subgrade reaction, k, is inputed by a data variable SREAC. The loss of contact behavior of the slab with the soil is modeled as follows:

- The Gauss point displacement, GDISP, of a particular Gauss point of the slab element is checked.
- If GDISP > 0, then that Gauss point is assumed to uplift and lose contact with the subgrade. Hence, the contribution of that Gauss point to the stiffness matrix calculation as well as in the equivalent nodal force vector calculation is not taken into account.
- If GDISP ≤ 0, i.e., the Gauss point is still in contact with the subgrade. Hence, its contribution to the stiffness matrix and equivalent nodal force vector calculations is taken into account.

The above steps are summarized as follows:

$$GDISP = \begin{cases} \leq 0 & \text{Gauss point displaces down} \\ > 0 & \text{Gauss point displaces up} \end{cases}$$

Moreover, every problem of a slab on an elastic foundation is solved initially, i.e., for the first iteration of the first increment, by assuming full contact of slab with the subgrade.

The introduction of cavities or sinkholes in the model WINKLER is controlled by the variables NELCAV, NELCV and IGPCOD. The parameter NELCAV represents the total number of elements over a cavity, NELCV represents the particular element number, and IGPCOD is the cavity code describing the number of Gauss points of that element which rest over the cavity. This feature of the model enables the modeling of any shape or size of cavity that lies underneath the slab.

6.2.3 Sequential Operation

The flow of operations of program WINKLER is schematically shown in Figure 6.1.

6.2.4 Subroutines

In this section all the subroutines used in the model WINKLER are briefly explained below. They are listed alphabetically:

ALGOR The equation resolution index, KRESL is determined depending on the choice of non-linear solution algorithm.

BGMAT The strain-displacement matrix [B] is evaluated at each Gauss integration point of each layer of all elements, before entering into the incremental and iterative loops. The shear terms are evaluated at four Gauss points and are extrapolated to nine Gauss points. The [B] matrix is written on a TAPE in the sequence of elements and layers for later use avoiding the recalculation

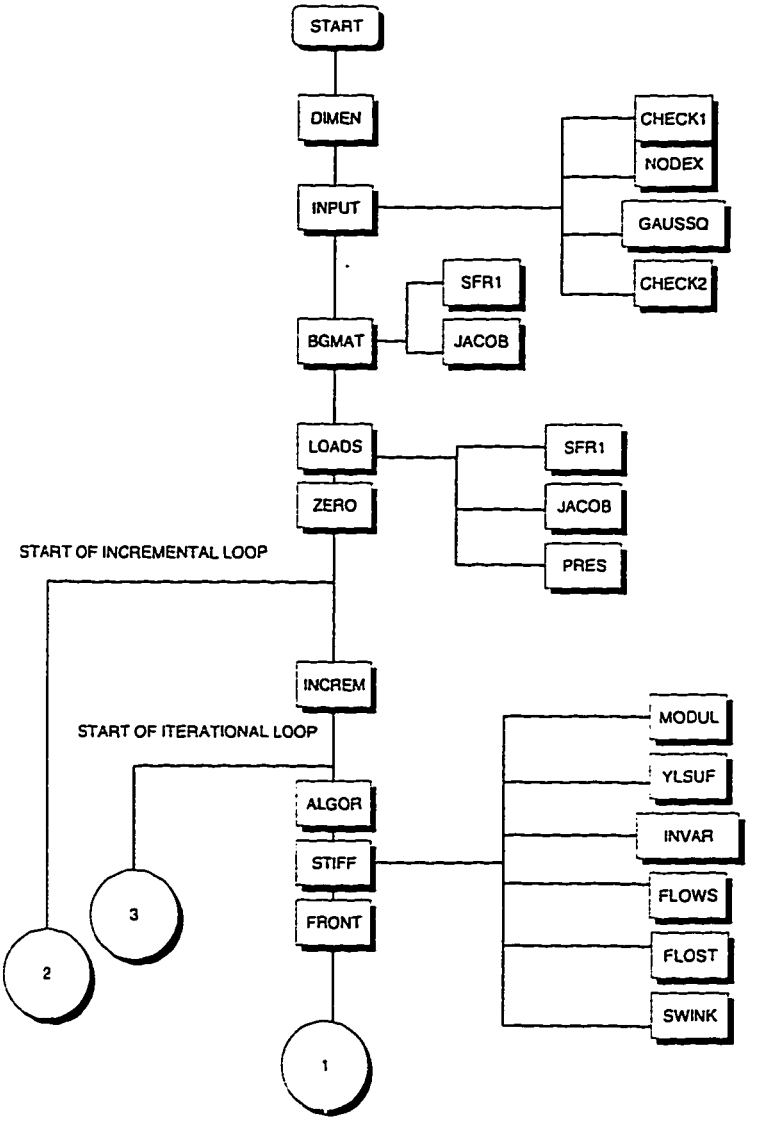

Figure 6.1: Flowchart for the WINKLER Model (contd...)

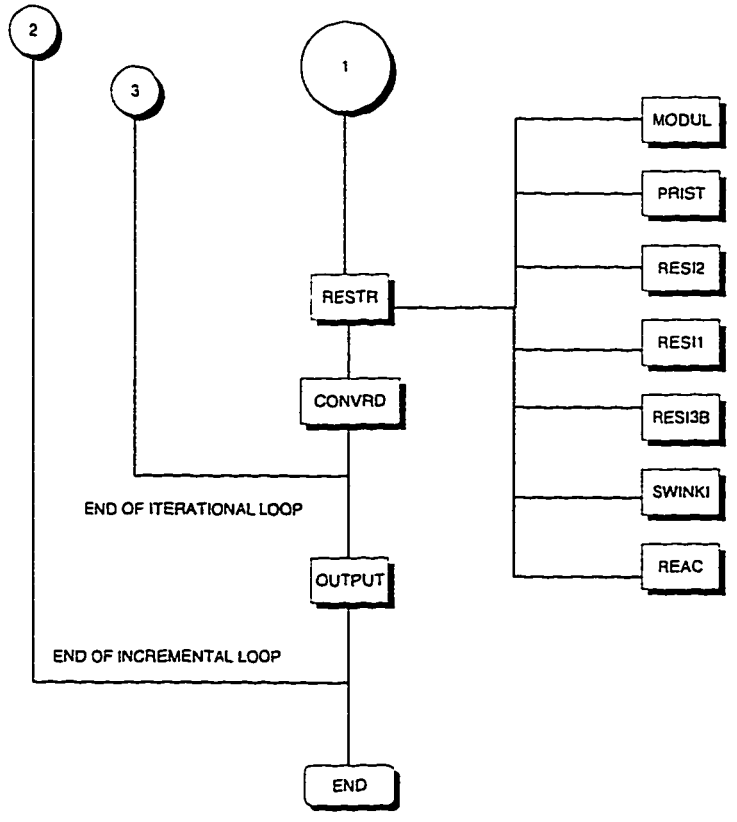
2
3
1
MODUL
PRIST
RESI2
RESTR
RESI1
CONVRD
RESI3B
SWINKI
END OF ITERATIONAL LOOP
OUTPUT
REAC
END OF INCREMENTAL LOOP
END

each time.

CHECK1 Diagonizes a part of the already read data for verification before actually entering into the analysis procedure.

CHECK2 Verifies the remaining data after the subroutine CHECK1.

CONVRD Checks the convergence criteria using the displacement norm.

DIMEN The maximum dimensions are defined for the program in the beginning and are passed to all subroutines as arguments. It helps in minimizing the chance of errors related to dimensioning the arrays.

ECHO If data errors have been detected by subroutines CHECK1 or CHECK2, this subroutine reads and writes the remaining data cards.

FLOST Calculates the flow vectors using Von Mises yield criteria.

FLOWS Calculated the flow vectors for different yield criteria.

FRONT Uses the frontal solving technique for solving symmetric positive definite matrices (exclusively for solving the equations related to slab)

GAUSSQ Sets-up the Gauss-Legendre sampling positions and weights.

INCREM Reads the load increment data and updates the loads, the tolerance value, the maximum iteration number and the control parameter for optional output.

INPUT Reads most of the input data needed for the start of the analysis such as the control parameters defining various options, element, and layer discretization; material properties; and boundary conditions.

INVAR Evaluates the stress invariants and the value of the yield function using different yield criteria.

JACOB Evaluates the Jacobian matrix and the shape function derivatives.

LOADS Reads the control parameters to identify the types of loading applied and then calculates the consistent nodal forces due to each type of the given loads.

MODUL Calculates the elasticity matrix in the local axis system.

NODEX Generates the coordinates of midside nodes using the given coordinates of corner nodes.

OUTPUT Displays the selective output depending upon the options read as control parameters in the subroutine INCREM.

PRES Evaluates the nodal loads if any of the elements are uniformly distributed.

PRIST Calculates the principal stresses in the structural plates or slabs.

REAC Calculates the net subgrade reaction and the contact area of the slab with the subgrade.

RESI1 Calculates the residual stresses for the uncracked concrete.

RESI2 Calculates the residual stresses for the cracked concrete.

RESI3B Calculates the residual stresses for the steel layers.

RESTR Most important subroutine of the non-linear elasto-plastic iterative incremental computational algorithm. Reduces the stresses, and eventually the equivalent nodal forces are evaluated, which are statically equivalent to the corrected stresses. The difference of the applied nodal loads and the equivalent nodal loads results in the residual forces which are reduced in successive iterations to a tolerable value to meet the desired degree of convergence in the subroutine CONVRD.

SFR1 Generates shape functions and their first derivatives for the selected element type at any given value of natural coordinates at sampling points.

STIFF Evaluates the stiffness matrix for each element in turn. The process involves the reading of strain matrix [B] as given by subroutine BGMAT and then the evaluation of [D] matrix as given by subroutine MODUL, depending upon the state of material as elastic, cracked or elasto-plastic. Using [B] and [D] the element stiffness matrix [K] is evaluated by performing numerical integration within the layers and summation through the thickness over all layers. Output is written on a TAPE in the sequence of element numbers for later use.

SWINK Special subroutine for the Winkler model. Evaluates the subgrade stiffness matrix by making use of the modulus of subgrade reaction, k.

SWINKI Similar to subroutine SWINK, but to be specifically used in the subroutine RESTR.

YLSUF Updates the yield stress and the strain hardening parameter.

ZERO All the arrays of stresses, strains, effective stresses, effective plastic strains and directions of cracks are initialized to zero at the beginning.

6.3 Program PSUEDO-3D

In this section the main programming features of the Program PSEUDO-3D are described, based on the theoretical formulation given in Chapter 5.

6.3.1 Material and Finite Element Parameters

The material and finite element parameters for the model PSEUDO-3D includes the following in addition to those described in Section 6.2.1.

An elastic model is used to model the soil, where the soil is defined by the Young's modulus of elasticity (E_{soil}) and the Poisson's ratio of soil (ν_{soil}). A three dimensional hexahedral brick element, with a total of 27 nodes and three degrees of freedom at each node is used to model the soil. Due to the elastic behavior of

the soil, the stiffness matrix $[S_{3d}]$ is calculated only once in the first iteration of the first increment and therefore requires no updating. A normal integration scheme ($3 \times 3 \times 3$) is employed to evaluate the element stiffness matrix. The boundary conditions for the elastic soil are specified by the three translations u, v, and w in the x, y, and z directions, respectively.

6.3.2 Evaluation of the Equivalent Subgrade Modulus

In the model WINKLER, a displacement criteria is used to model the loss of contact phenomenon; whereas in PSEUDO-3D model, a stress-based criteria is employed to model the same phenomenon. In the later case, the vertical stresses in the top layer of the soil mass are monitored. If the stresses are tensile, then the loss of contact phenomenon is taken into account. For a slab on an elastic soil in the model PSEUDO-3D, a vertical force equilibrium is made the criteria for convergence.

One important point in the discretization phase of the slab and the soil is that, the slab and the soil lying under the slab, are discretized into the same number and same size of finite elements. Also the node numbering order for that portion of soil underneath the slab must be similar to that of the slab.

The variable SREAC which describes the modulus of subgrade reaction remains a constant in the model WINKLER, but in PSEUDO-3D model it is inputed with an initial assumed value which is then re-calculated at different positions, depending on the stress and the vertical displacement of that point. The calculation of the

equivalent subgrade modulus for a non-linear analysis is controlled by a variable NALGO3. If NALGO3 is kept equal to '0' then the model calculates the equivalent subgrade modulus vector in each iteration of each increment: if it is equal to '1' then it calculates the vector of equivalent subgrade modulus only in the second iteration of each increment. As the vector of equivalent subgrade modulus remains the same for a load increment, this feature of the model helps in reducing the computing time during a non-linear analysis.

6.3.3 Sequential Operation

The flow of operations of program PSEUDO3D is schematically shown in Figure 6.2

6.3.4 Subroutines

The PSEUDO-3D program subroutines include the following in addition to those given in Section 6.2.4. These are listed alphabetically:

BMATP3 Evaluates the strain displacement matrix.

CHEK13 This subroutine checks the main control data.

CHEK23 Checks the remaining data after check by CHEK13.

DBE3 Multiplies the elasticity matrix [D] by the strain matrix [B].

DIMEN3 Presets the variables associated with dynamic dimensioning.

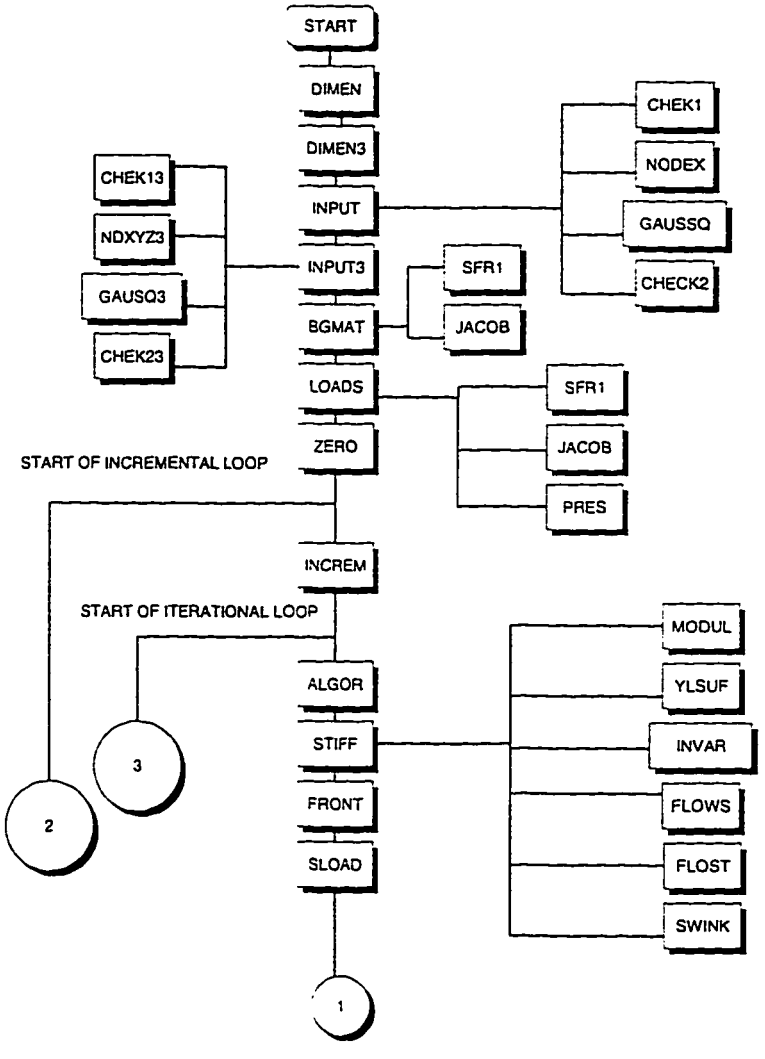

Figure 6.2: Flowchart for the PSEUDO-3D Model (contd...)

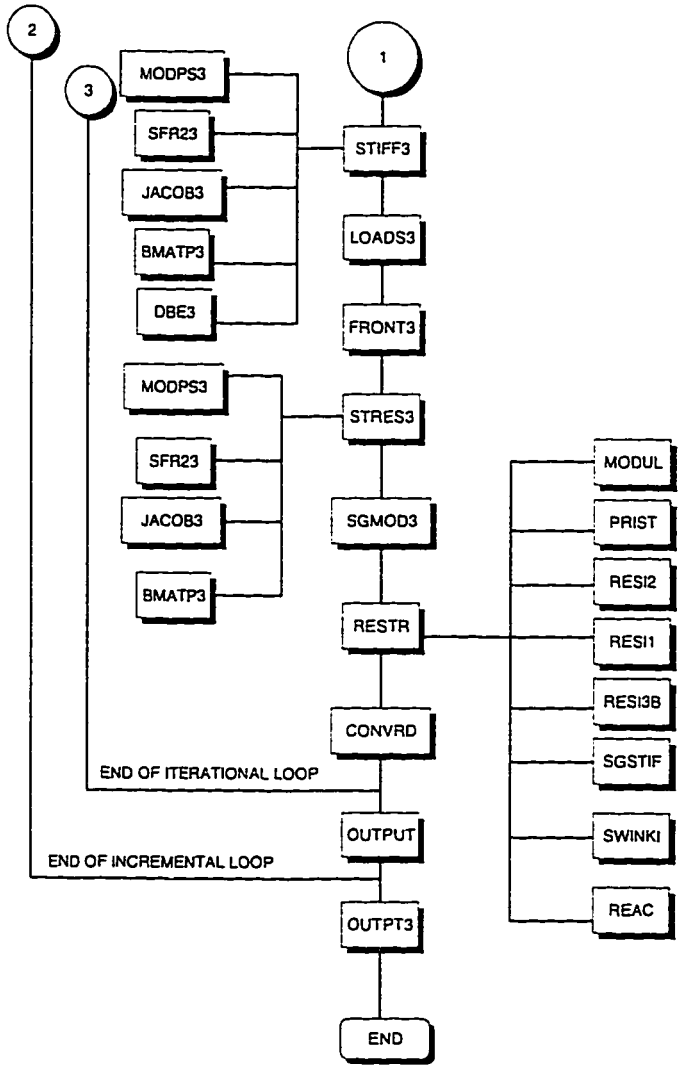
2
3
1
MODPS3
SFR23
JACOB3
BMATP3
DBE3
STIFF3
LOADS3
FRONT3
MODPS3
SFR23
JACOB3
BMATP3
STRES3
SGMOD3
RESTR
CONVRD
END OF ITERATIONAL LOOP
OUTPUT
END OF INCREMENTAL LOOP
OUTPT3
END
MODUL
PRIST
RESI2
RESI1
RESI3B
SGSTIF
SWINKI
REAC

ECHO3 If data errors have been detected by subroutines CHEK13 or CHEK23, this subroutine reads and writes the remaining data cards.

FRONT3 Frontal solver for symmetric positive definite matrices.

GAUSQ3 This subroutine sets up the Gauss-Legendre integration constants.

INPUT3 Accepts most of the input data relevant to the three dimensional soil problem.

JACOB3 This subroutine evaluates the Jacobian matrix and the cartesian shape function derivatives.

LOADS3 Evaluates the consistent nodal forces for each element after reading the loading data.

MODPS3 Evaluates the elasticity matrix [D].

NDXYZ3 This subroutine interpolates the mid-side nodes of straight sides of elements and the central nodes.

OUTPT3 Outputs the displacements, reactions and stresses depending on the output parameter read in subroutine INPUT3.

SFR23 Evaluates the shape functions and their derivatives for the three dimensional hexahedral brick element.

SGMOD3 Calculates the new equivalent subgrade modulus at each Gauss point using the displacement vector and the stresses from the 3-D elements.

SGSTIF Calculates the subgrade stiffness matrix with the updated subgrade modulus values.

SLOAD This subroutine calculates the subgrade forces by using the subgrade stiffness matrix and the displacement vector.

STIFF3 Evaluates the stiffness matrix for each element in turn and writes the output on a TAPE in sequence of element numbers.

STRES3 Evaluates the stresses and the strains assuming a linear elastic behavior.

Chapter 7

RESULTS AND DISCUSSIONS

In this chapter some of the numerical examples that have been attempted for the verification of the proposed models are given. In addition, other new results involving the linear and non-linear responses of slabs on elastic subgrade are included. Load deflection curves, displacement profiles, and distributions of subgrade reaction coefficient resulting from the numerical problems that are tested using the two models WINKLER and PSEUDO-3D are also presented.

7.1 Problem Description

The slab used in the present numerical work is shown in Figure 7.1. The dimensions of the square slab are $2a \times 2a$ with a thickness of h. being centrally loaded with a patch load of size $l \times l$. For the Winkler case, the slab is assumed to be resting on

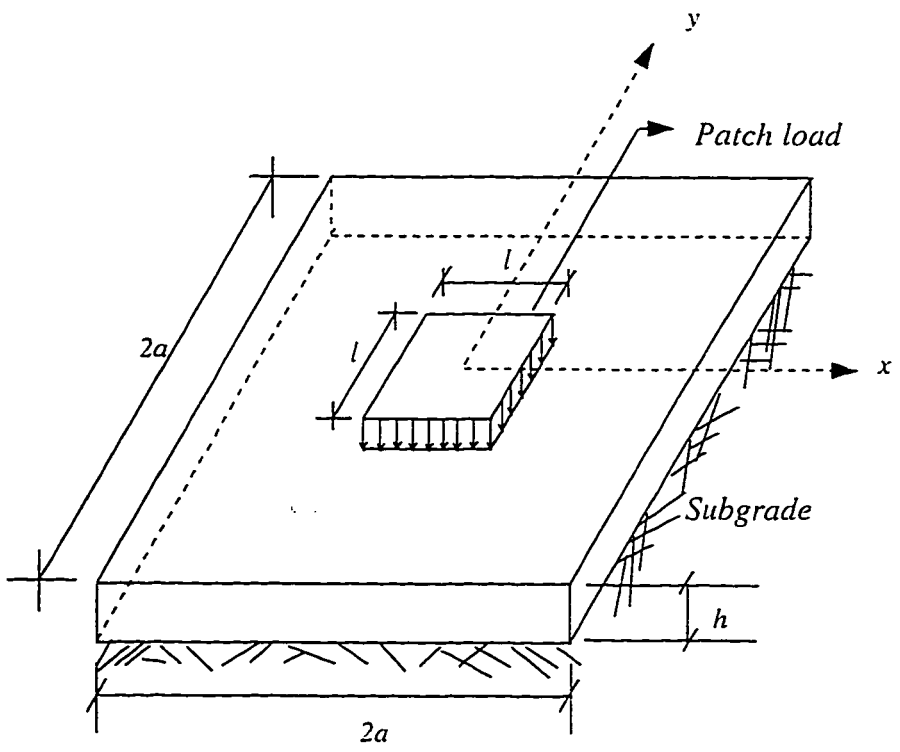

Figure 7.1: Square R/C Slab on Subgrade with Central Patch Load.

a subgrade soil of known uniform subgrade reaction, k. The flexural rigidity of the slab is defined by $D = (E_c h^3)/(12(1-\nu^2))$, where ν is the Poisson's ratio of the slab which is taken as zero and E_c is the modulus of elasticity of the concrete.

7.2 Verification of the Model

7.2.1 Elastic Behavior

In this section, a square thin plate loaded at the center and resting on a tensionless Winkler subgrade is investigated. Only one quarter of the total slab is used in the analysis, because of the symmetry of load and geometry about both the axes. The quarter slab model is discretized using a uniform mesh of 16 elements. The central element is loaded with a very small patch load, well below the level expected to cause any degradation in the slab, to gaurrantee elastic behavior. A dimensionless contact length of the slab with the subgrade is defined by (r/a), where r is the radius of the resulting circular contact region, and a is half the slab width.

Figure 7.2 shows the curves of dimensionless contact radius (r/a) versus the dimensionless relative stiffness parameter, $\lambda = (ka^4)/D$. The results from the present finite element model WINKLER are compared with that of Villaggio [11]. He employed the boundary element method for the determination of the contact region of a plate on an elastic foundation that reacts only in compression, when loaded with a concentrated load at the centre. An elliptic contact region for a case of rectangular

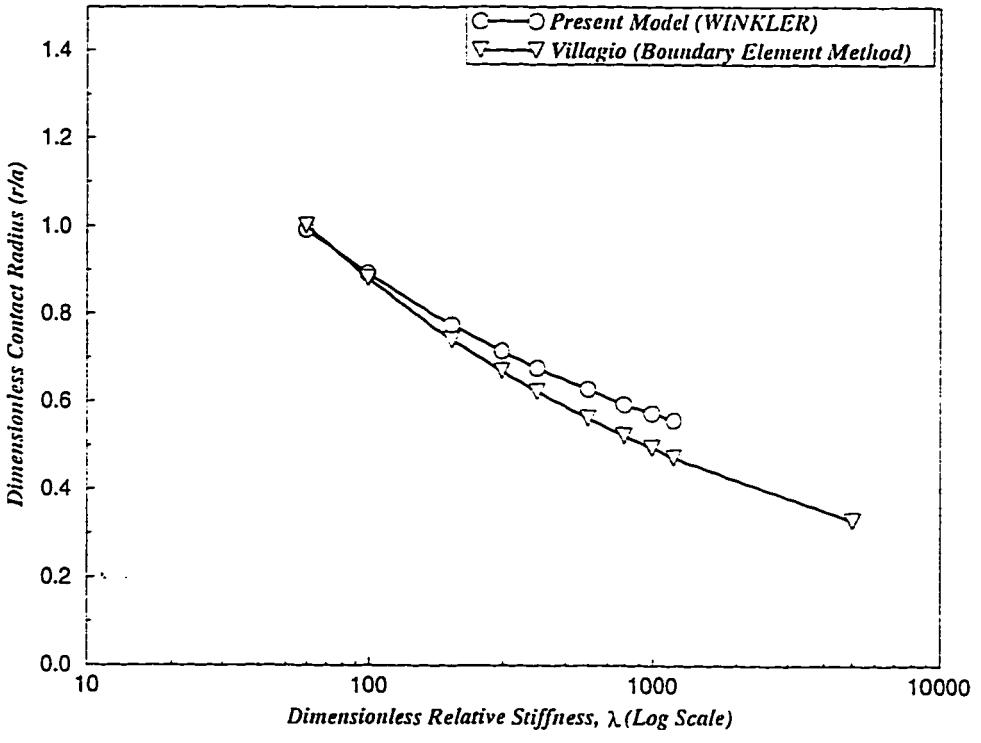

Figure 7.2: Comparison of Size of Contact Zone Dependence on the Relative Stiffness, λ.

plate was assumed in his approach. Even though in the present model a square slab is used with a patch load, rather than with a point load, the results still show a good agreement in predicting the contact region of the slab with the subgrade.

7.2.2 Inelastic Behavior

The non-linear capability of the present model (WINKLER) is tested to investigate the collapse of a column footing similar to the one which was used by Richart [31] in his experimental studies of reinforced concrete wall and column footings. Figure 7.3 shows the load-central deflection curve obtained using the present model (WINKLER) in comparison to the ultimate load values obtained by Richart as well as from the unfactored ACI design formula. The footing tested was of size $214cm \times 214cm$ and of $40.64cm$ thickness, with a central column of $30cm \times 30cm$. The following parameters were used in this case: $E_c = 2230kN/cm^2$, Reinforcement ratio, $\rho = 0.22\%$, Compressive strength of concrete, $f'_c = 2.18kN/cm^2$, Steel yield stress, $f'_y = 42.47kN/cm^2$. It should be noted that Richart tested the footing by placing it on equidistant elastic springs which resembles the Winkler model. In the present model a nominal value of $k = 0.02kN/cm^2$ is used to represent the subgrade. The ultimate load obtained from the present model is 1560 kN which is expectedly greater than the ACI design value. The numerical failure load prediction compared to the experimentally tested footing shows excellent agreement, which indicates the validity of the numerical approach.

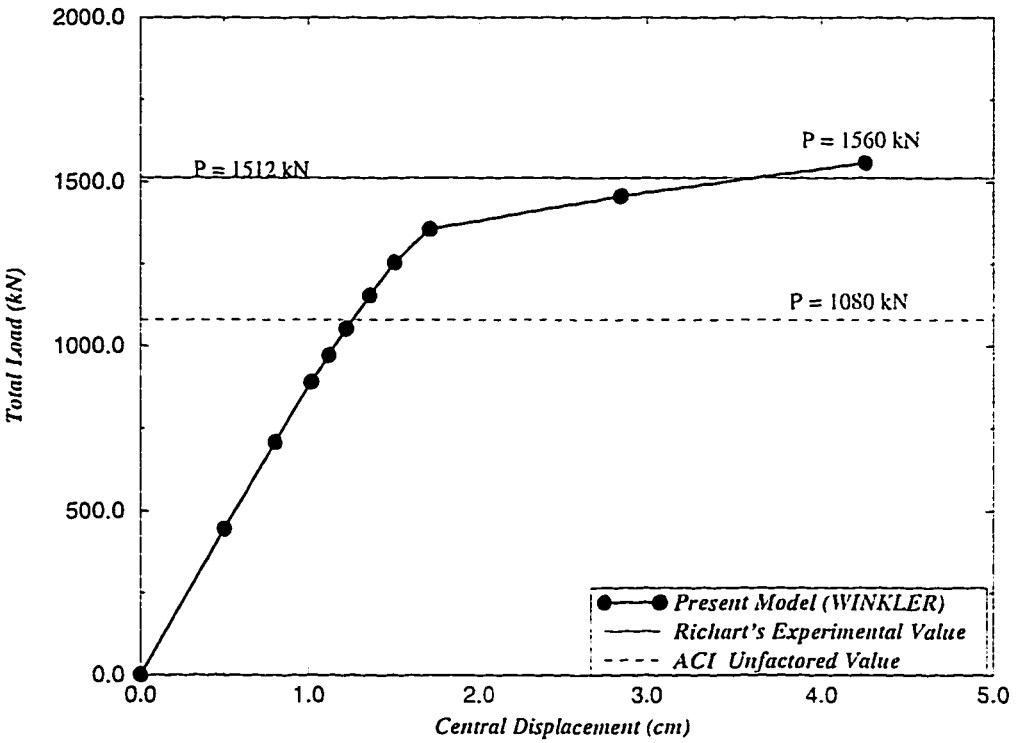

Figure 7.3: Load - Central Deflection Curve in Comparison to Richart's Experimental Failure Load and ACI.

7.3 Winkler Model - Cavity Effect

7.3.1 Effect of Cavity Size

Figure 7.4 shows a quarter model of the slab used in predicting the failure loads of a slab with an underlying cavity of variable size. Four cavity sizes are considered, with a non-changing central patch load over the first element. Since the cavities and the applied load are symmetric about both the axes, only one quarter of the slab is used in the analysis. The slab dimensions are given by: $2a = 400cm$, $h = 80cm$, $E_c = 2150kN/cm^2$, $f'_c = 2kN/cm^2$, $E_s = 20000kN/cm^2$, $f_y = 40kN/cm^2$, $\rho = 0.22\%$. The patch load size is given by $l = a/2 = 100cm$. The subgrade soil is represented by a soft Winkler subgrade with $k = 0.01kN/cm^3$.

The ultimate loads for the slab with four cavity sizes and without cavity considered for the size effect study are given in Table 7.1. Comparing the failure load of the slab without cavity to that of cavity IV, there is a decrease of about 21%, which proves that the cavity size has a significant impact on the failure load of RC slabs on subgrade.

Figures 7.5 and 7.6 show the load deflection curves for the central node A, and the corner node B, in addition to the unfactored design value of the ultimate load as given by the ACI code. The load deflection curves for the same slab without any cavity are also indicated. As expected, the failure load of the slab without cavity is greater than the remaining four cases. For cavity I & cavity II there is not much

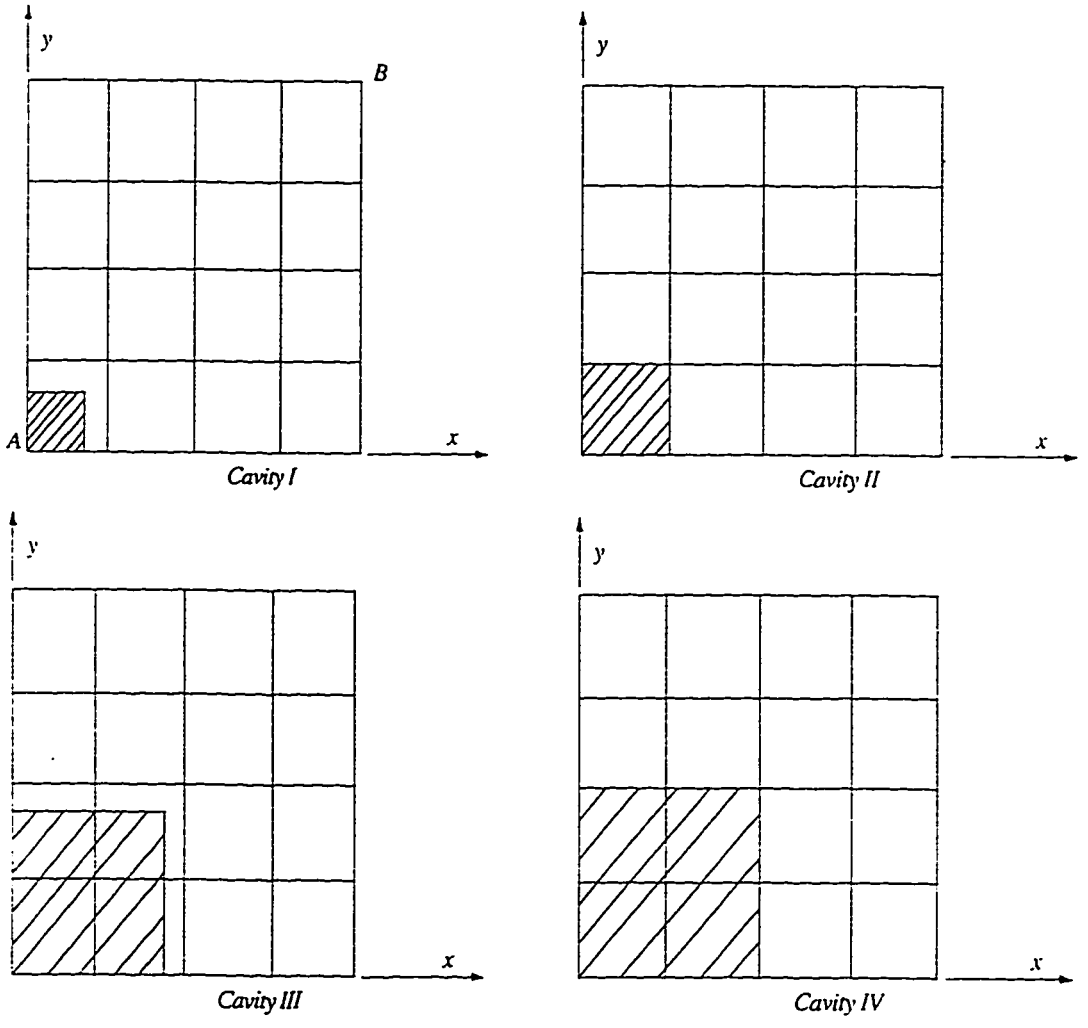

Figure 7.4: Four Cavities considered for the Cavity Size Effect Study.

Table 7.1: Ultimate Loads for Four Cavities and without Cavity Considered for the Size Effect Study.

Cavity Type	*Cavity Area* (cm^2)	*Ultimate Load* P_u *(kN)*
No Cavity	0	5760
I	5216	5460
II	10000	5460
III	29660	4740
IV	40000	4560

difference in the failure loads which can be attributed to the cavity size, since for these two cases the loaded area, i.e. patch area, is either greater or equal to the size of the cavity. Interestingly, the failure load for cavity III & IV is less than the value given by the ACI code, which clearly shows the critical nature of the failure load prediction from the ACI code. Also, the two curves corresponding to cavity I & cavity II, exhibit more ductility compared to the remaining two cases.

From Figure 7.6, for the same curves there is a greater lift-off of the corner node B, as can be noticed in the reversal of sign of the corner deflection along the X-axis. The reversal in the deflection of the corner in the first three cases indicates the development of a flexural collapse mechanism. In contrast, the cases involving larger cavities exhibit a behavior indicative of punching shear failure.

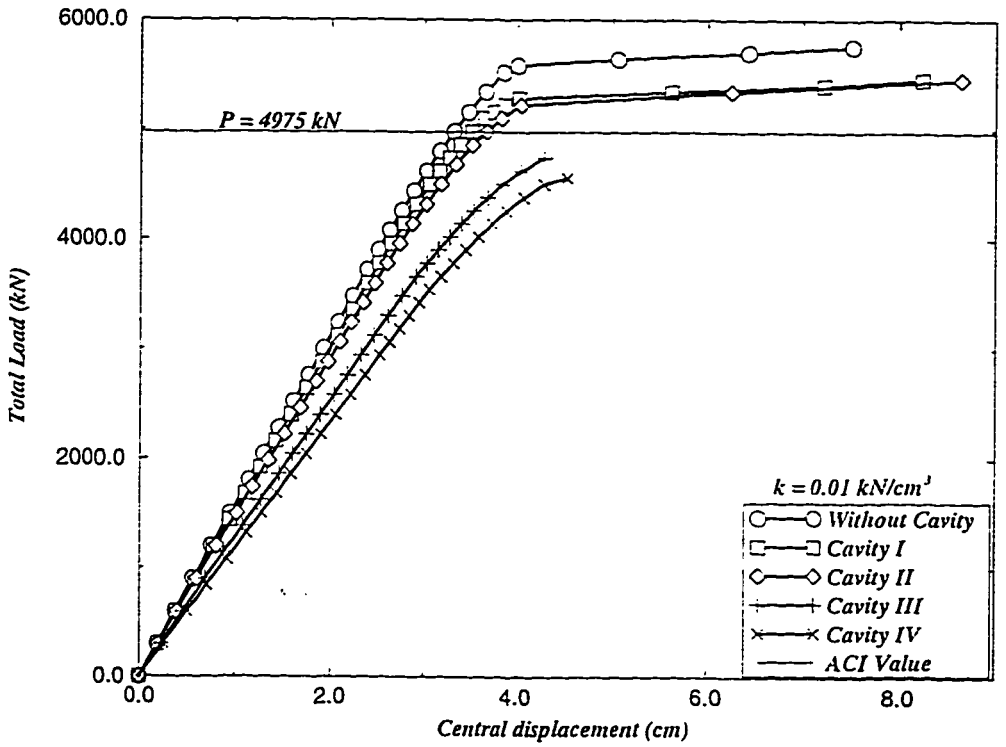

Figure 7.5: Load - Central Deflection (Point A) Curves for a Slab with Cavities I, II, III & IV and without a Cavity.

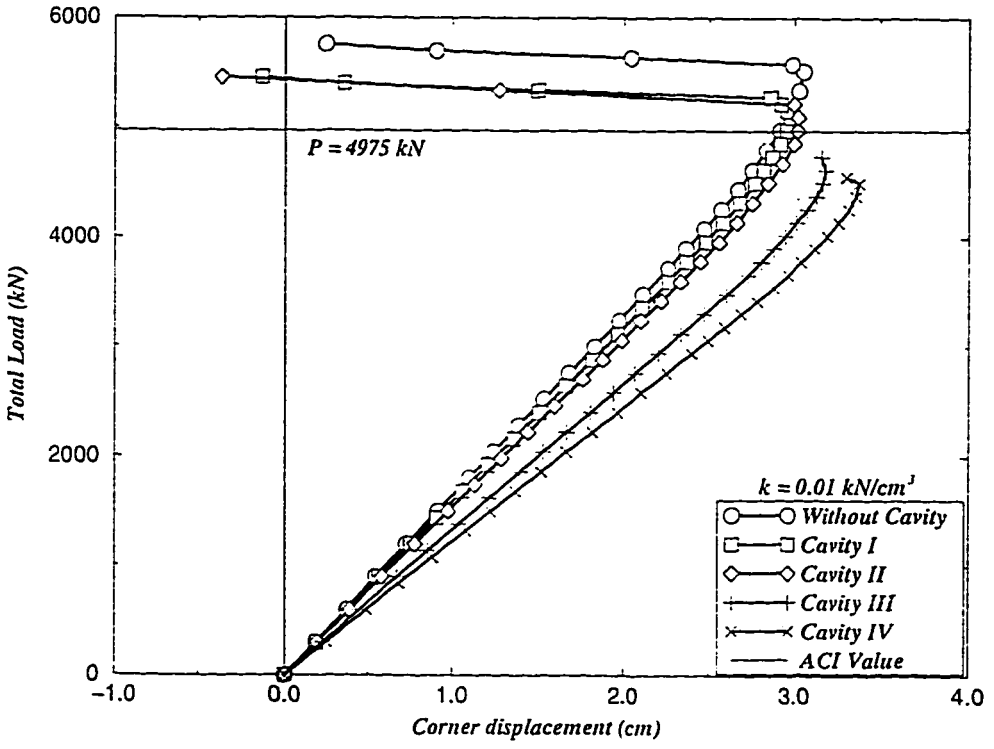

Figure 7.6: Load - Corner Deflection (Point B) Curves for a Slab with Cavities I, II, III & IV and without a Cavity.

7.3.2 Effect of Cavity Location

The effect of location of the cavity on the failure loads is investigated for the same slab as given in Section 7.3.1 but with a $\rho = 0.32\%$ and two different subgrade moduli $k = 0.01kN/cm^3$ and $k = 0.1kN/cm^3$. Three locations of the cavity (Figure 7.7) are considered. The cavities considered are symmetric over half of the slab, hence one-half of the slab is used for the evaluation of the failure loads. The applied patch load is the same as given in Section 7.3.1., and remains at the slab geometric center.

For a soft subgrade ($k = 0.01kN/cm^3$), the cavity location does not show any significant effect on the capacity of the slab, which is seen from the ultimate load values given in Table 7.2. In Contrast, for a stiffer subgrade ($k = 0.1kN/cm^3$), the cavity location showed some significant effect on the capacity of the slab.

Load deflection curves for the central node A and the corner node B are given in Figure 7.8 through Figure 7.11. A little effect on the central displacement (Point A) is seen(Figure 7.8). For the same subgrade, the corner node B showed a loss of contact behavior (Figure 7.10). In addition, Cavity III, shows relatively more loss of contact in comparison to cavities I & II, and all the three cases show the loss of contact behavior at the same load level. The effect, as seen in Figure 7.8 and Figure 7.10, of a soft subgrade can be attributed to the distribution of pressure under the slab. The pressure is more or less distributed uniformly all over the contact area of

Table 7.2: Ultimate Loads for Cavities I, II, & III for $k = 0.01 kN/cm^3$ and $k = 0.1 kN/cm^3$

	k = 0.01 kN/cm^3			k = 0.1 kN/cm^3		
Cavity	I	II	III	I	II	III
Ultimate Load P_u (kN)	5390	5390	5460	5530	5810	6230

the slab with the subgrade.

For a stiff subgrade, Cavity III showed a relatively ductile type of failure (Figure 7.9). The corner node B showed significant loss of contact for all the three cavity types (Figure 7.11) and at different load levels. The increase in the distance between the cavity and the load, results in greater lift-off of the corner node B. The contrasting behavior of the stiffer soil as compared to the soft soil is due to the concentration of subgrade pressure distribution towards the location of the loading. This can be seen from the different ultimate loads for the three cavity locations (Table 7.2). The redistribution of pressure towards the centre of the slab as the cavity moves away from the centre actually increases the capacity of the slab.

The displacement profiles along the X-axis at the failure loads for both the soft and stiffer subgrades are shown in Figure 7.12 and Figure 7.13. A conical flexural failure mechanism is seen for cavity I on soft subgrade (Figure 7.12). As the cavity moved away from the load (for cavities II and III), the displacements under the cavity increased at a greater rate. For the slab on stiff subgrade (Figure 7.13) the displacement profiles for cavity I and II showed a similar flexural failure mechanism.

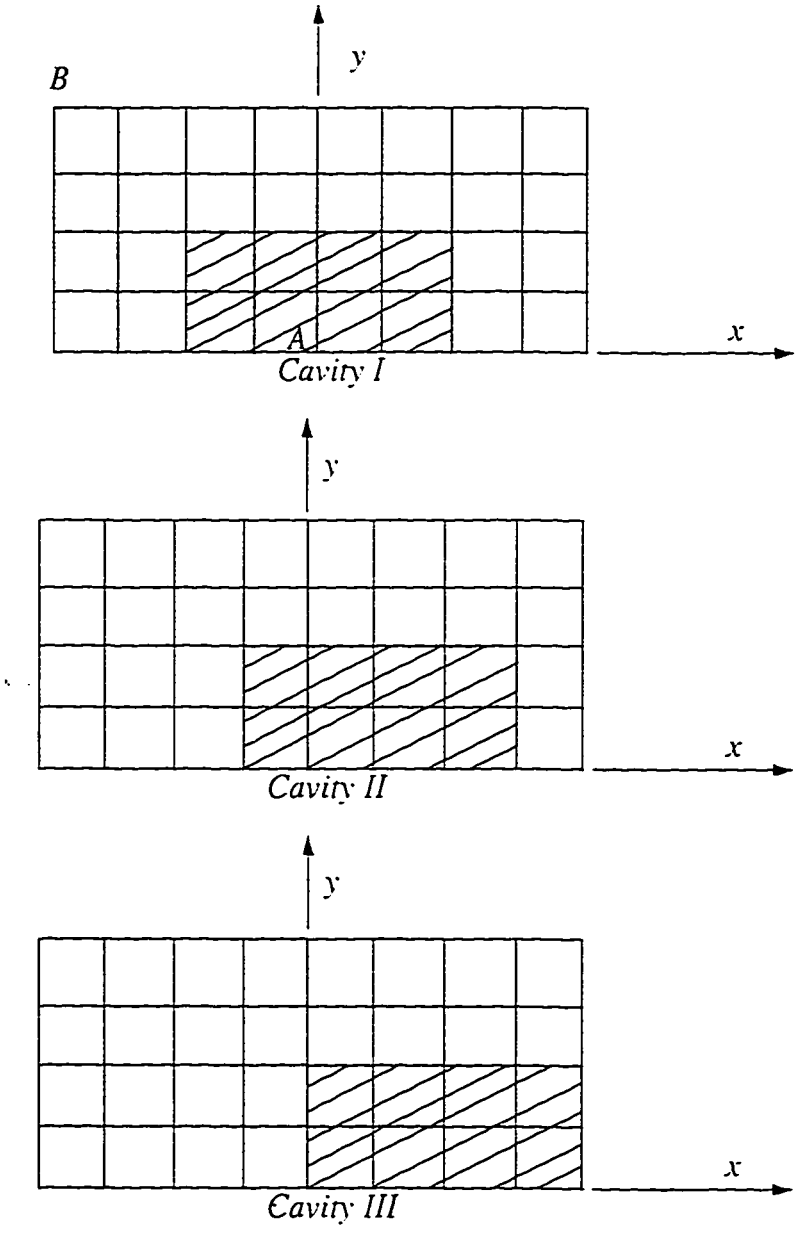

Figure 7.7: Type of Cavities Considered for the Cavity Location Effect Study.

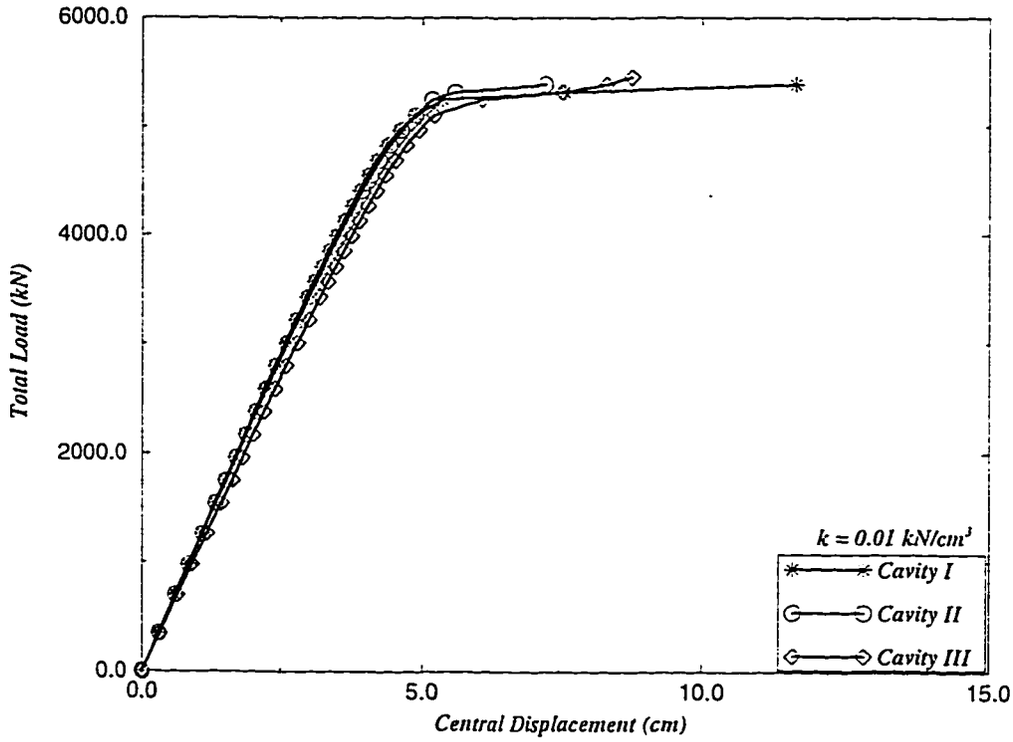

Figure 7.8: Load - Central Deflection (Point A) Curves for a Slab with Cavities I, II, & III and with $k = 0.01 kN/cm^3$.

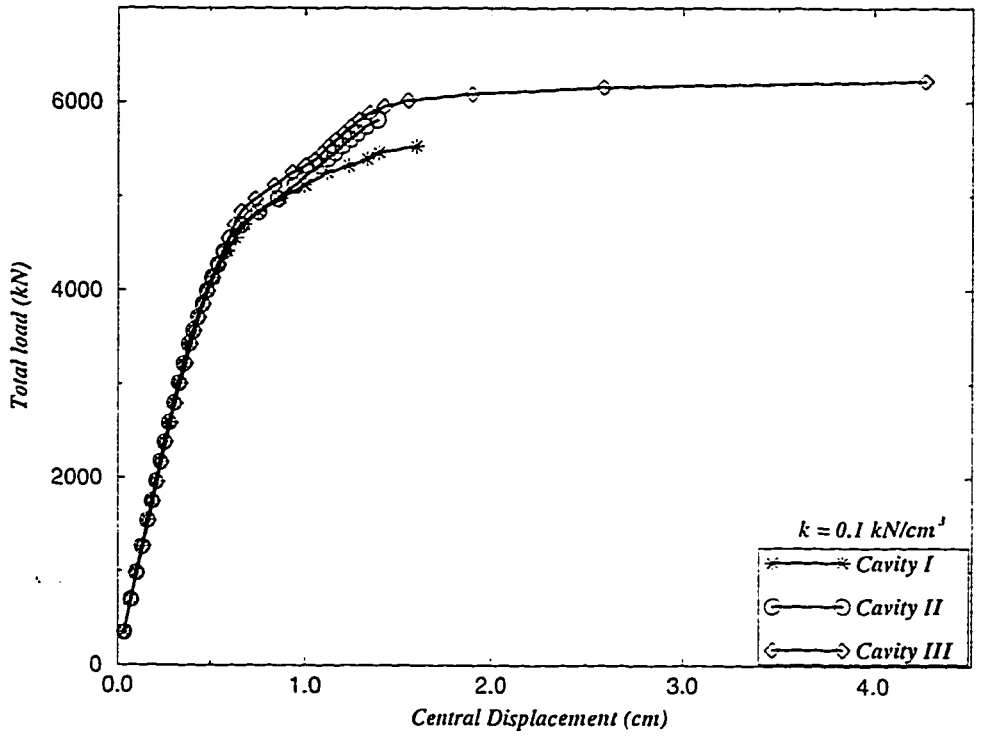

Figure 7.9: Load - Central Deflection (Point A) Curves for a Slab with Cavities I, II, & III and with $k = 0.1kN/cm^3$.

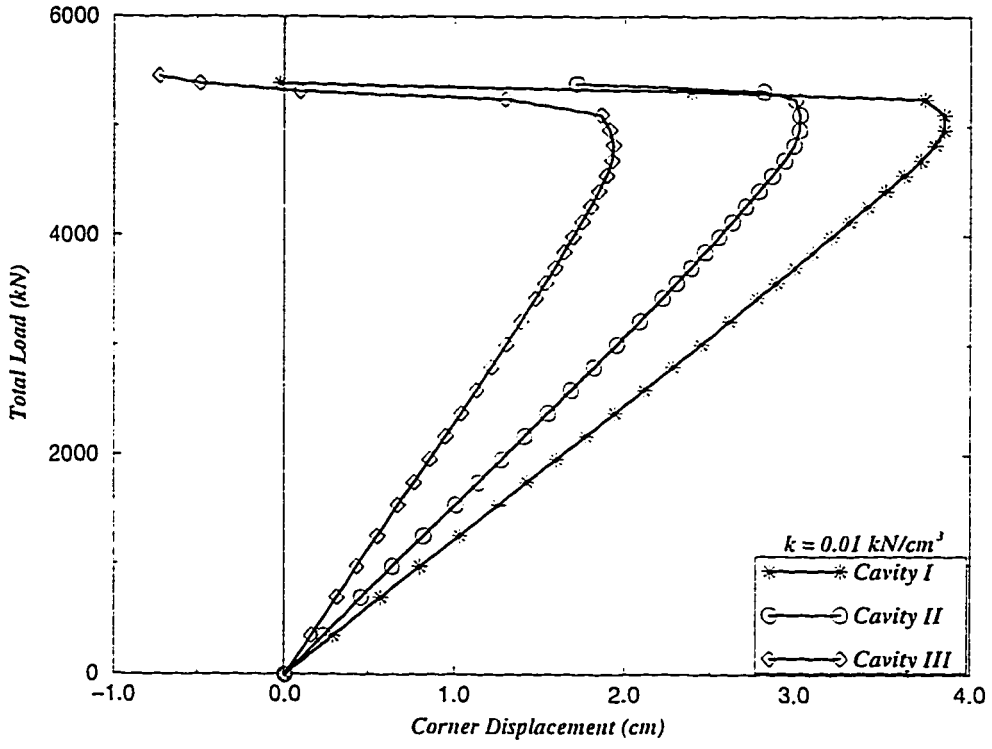

Figure 7.10: Load - Corner Deflection (Point B) Curves for a Slab with Cavities I, II, & III and with $k = 0.01 kN/cm^3$.

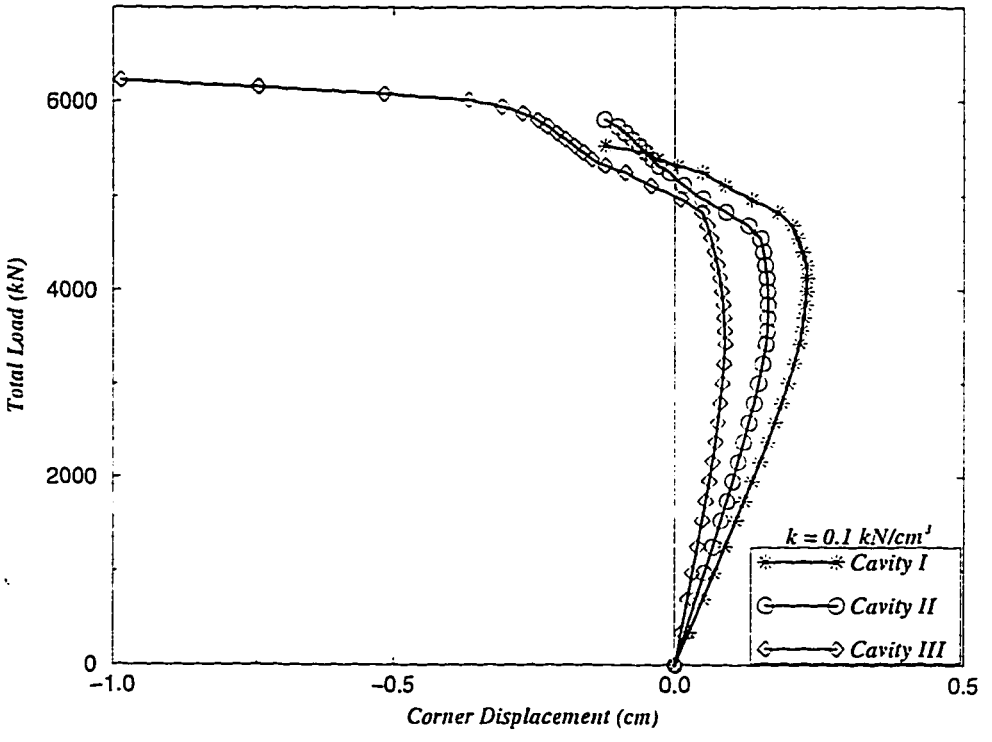

Figure 7.11: Load - Corner Deflection (Point B) Curves for a Slab with Cavities I, II, & III and with $k = 0.1kN/cm^3$.

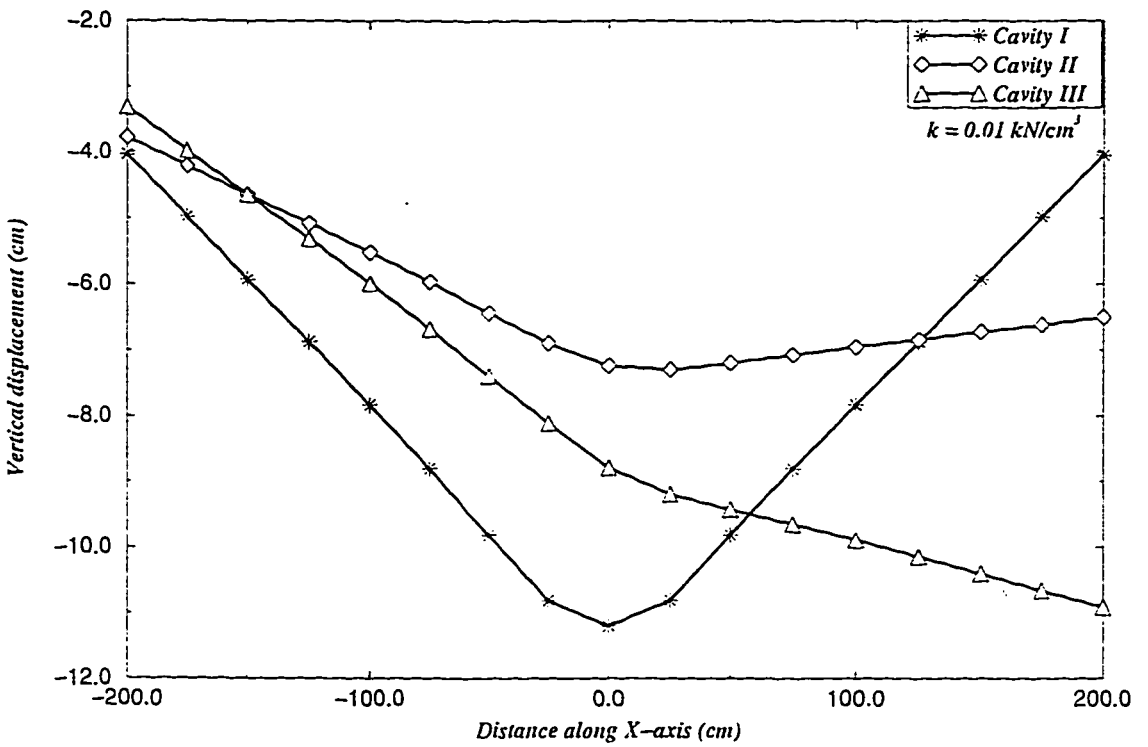

Figure 7.12: Displacement Profile along X-axis for a Slab with Cavities I,II, & III at the Ultimate Loads of each and with $k = 0.01 kN/cm^3$.

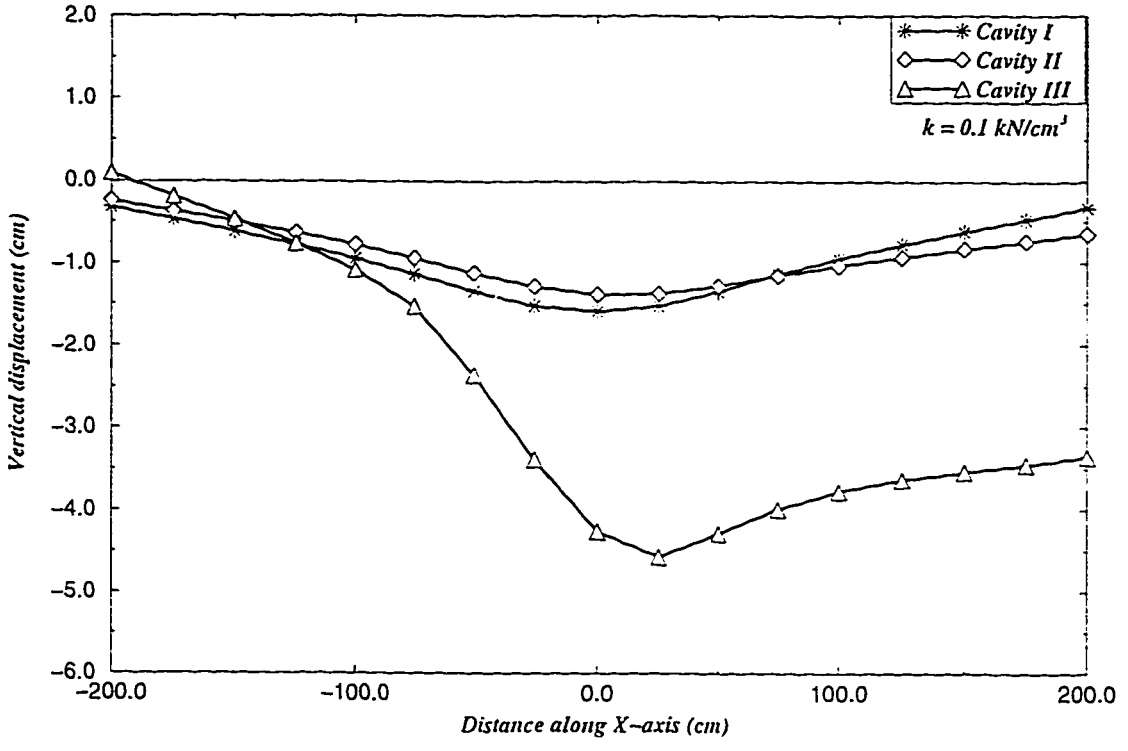

Figure 7.13: Displacement Profile along X-axis for a Slab with cavities I,II, & III at the Ultimate Loads of each and with $k = 0.1kN/cm^3$.

For a stiff subgrade, Cavity III showed a total uplift of the left edge, as the cavity is at the other extreme opposite edge of the slab.

7.4 PSEUDO-3D Model - Elastic Analysis

In this section, the problem of a square slab that rest on a large three dimensional elastic soil medium, is investigated. The slab geometry is the same as indicated in Figure 7.1, with only the Winkler subgrade replaced by the soil medium.

7.4.1 Geometry Description

Figure 7.14 shows a one-quarter model of a square slab resting on a large soil medium. The soil stiffness is defined by its modulus of elasticity, E_{soil}, and the Poissons ratio ν_{soil}, (taken as 0.3 for all cases). The soil considered is an elastic hexahedran with dimensions: $6a \times 6a \times 3a$, where a is half the slab width. The slab dimensions are $2a \times 2a$ and the thickness is given by h. The load is given by a central patch load of size $a/2 \times a/2$. For the quarter model considered, the analysis is carried out by discretizing the soil into 576 three dimensional elements, and the total number of nodes for the soil is 5491 with the total number of degrees of freedom equal to $5491 \times 3 = 16473$. The ratio of slab width to the soil width is kept equal to 3, so as to nullify the effect of boundary of the soil on the behavior of the slab itself. The vertical displacements of the bottom layer of the elastic soil

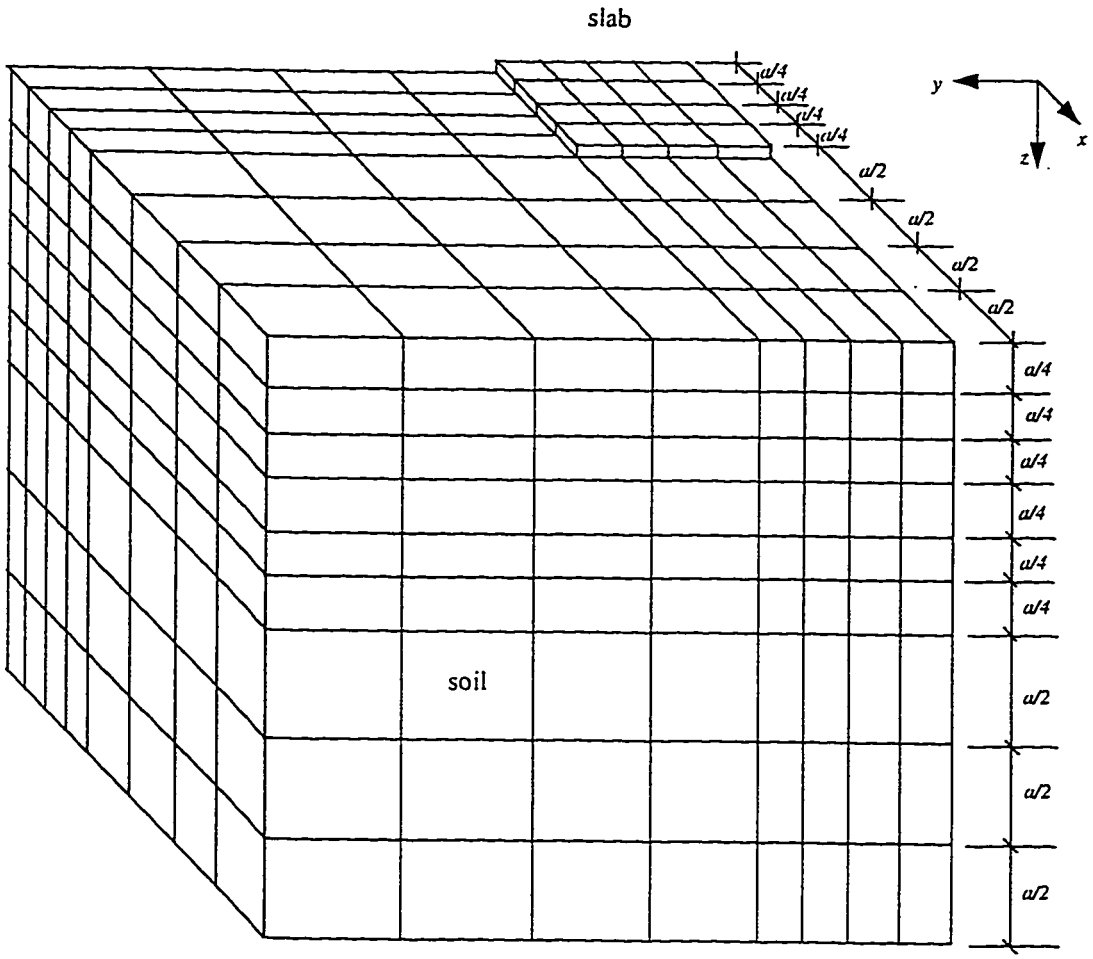

Figure 7.14: Quarter Model of Slab on a Three Dimensional Elastic Soil.

medium are restrained in the z-direction. The displacements in the y-direction and x-direction are restrained for the two symmetric sides $y = 0$, and $x = 0$, respectively. The other two sides of the elastic soil are modeled as free surfaces where there are no restraint for the displacements in x, y, and z directions. A non-dimensional relative stiffness parameter $\overline{\lambda}$, is defined for the soil and slab system and is given by $\overline{\lambda} = (E_{soil}a^3)/(2D)$, where D is the flexural rigidity of the slab.

7.4.2 Comparison of PSEUDO-3D and WINKLER Model

A square slab with a central patch load on a tensionless soil ($\overline{\lambda} = 670$) is analyzed using the PSEUDO-3D model and the same slab resting on Winkler subgrade of arbitrary k, is analyzed by the WINKLER model. The vertical displacement profiles from both the models are shown in Figure 7.15. For the cases analyzed by the WINKLER model, three values of λ which under-estimate, over-estimate and closely matches the central displacements of the PSEUDO-3D model are selected. From Figure 7.15, it can be concluded that all the three cases of WINKLER model over-estimate the edge displacements and under-estimate the radius of the contact region. In addition, the contact region for the three values of λ are different from each other. This shows the sensitivity of the WINKLER model to the selected value of subgrade reaction, k since each value of k produces its own unique solution. Hence, the use the PSEUDO-3D model in predicting the realistic behavior of the slab displacement and the contact zone is rightly justified and is much more advantageous.

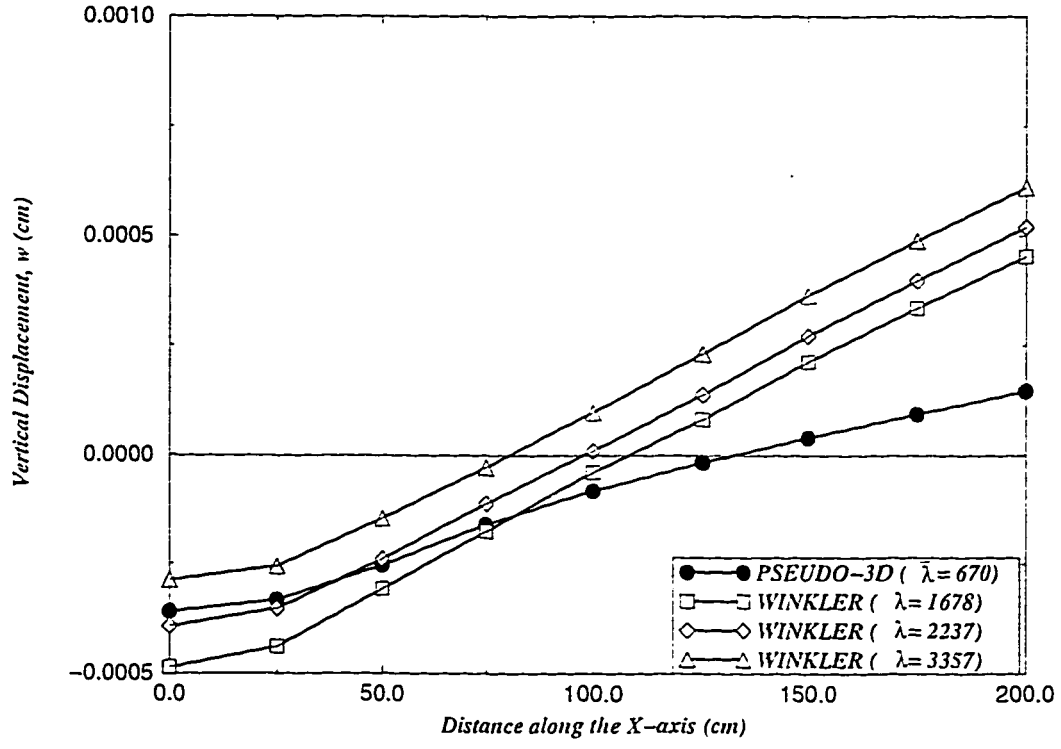

Figure 7.15: Comparison of Results of PSEUDO-3D Model and WINKLER Model.

7.4.3 Convergence Phenomenon

In this section, the elastic behavior of a slab on soil is investigated using the PSEUDO-3D model. As discussed in Chapter 4, several iterations are needed for the solution to converge, even in the elastic range, due to the nature of the adopted algorithm. A square slab with a central patch load on a soft soil ($\overline{\lambda} = 1.675$) is analyzed by PSEUDO-3D model. The convergence pattern of the independent normalized vertical displacements of the slab and the soil, for different iterations, is shown in Figure 7.16. The normalized vertical displacements are given by $\overline{w} = (wE_{soil})/(p_{avg}a)$, where E_{soil} is the modulus of elasticity of the soil, p_{avg} is the average pressure applied on the total slab, a is half the slab width, and w is the vertical displacements of the slab. For the case of patch loading, p_{avg} is calculated by distributing the patch load over the whole domain of the slab.

For the first iteration the slab and the soil displacements are unsurprisingly very much different from each other. This can be explained by the fact that the slab behaves independently from the soil in the first iteration. In the second iteration the effect of the soil is used to obtain a more accurate estimate of the value of the equivalent subgrade modulus k. This has led to a better agreement between the soil and the slab displacements. This process continues until the vertical equilibrium and displacement compatibility are almost satisfied which is given by the final iteration curves in the Figure 7.16.

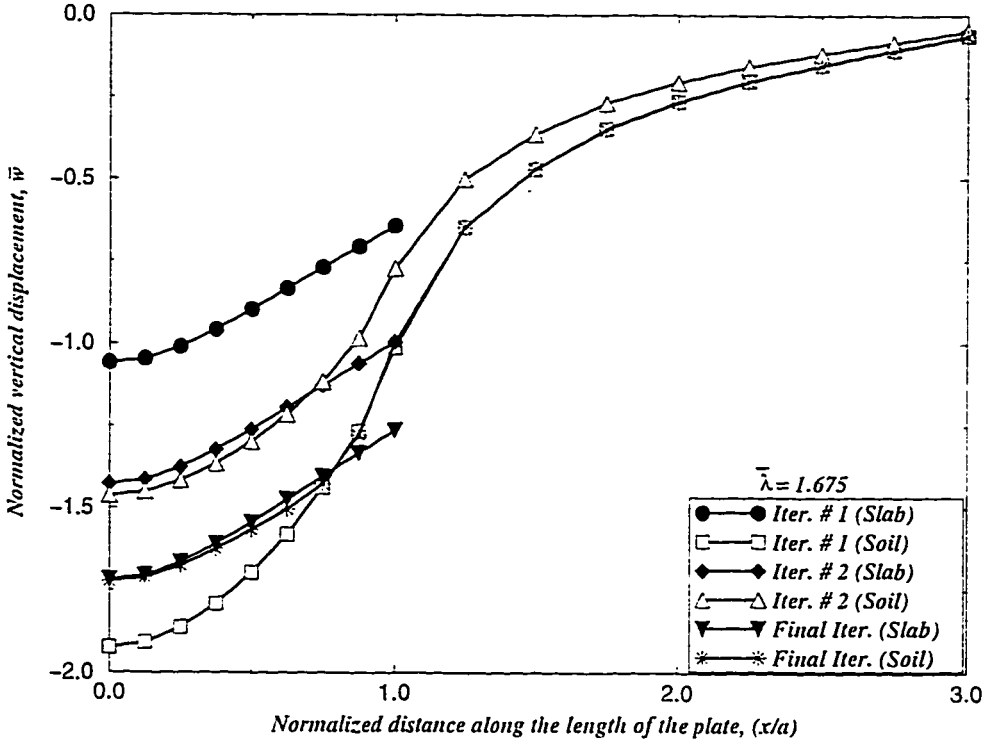

Figure 7.16: Convergence Sequence of the Slab Displacements and Soil Displacement for Different Iterations.

7.4.4 Elastic Deformations

Four different cases of a slab resting on a soil with variable stiffness, and subjected to patch loading or uniformly distributed loads, have been analyzed using the PSEUDO-3D model to study the behavior of the slab-soil system. The cases are: *CaseA* with $\overline{\lambda} = 1.675$ and patch loaded, *CaseB* with $\overline{\lambda} = 1675$ and subjected to uniformly distributed load, *CaseC* with $\overline{\lambda} = 16.75$ and patch loaded, *CaseD* with $\overline{\lambda} = 1675$ and subjected to patch loading. The three selected values of $\overline{\lambda}$ (1.675, 16.75, 1675) correspond to weak, intermediate and stiff soils, respectively.

The normalized displacement profiles for both the soil and slab for each of the four cases are shown in Figure 7.17 to Figure 7.20. From these figures it can be concluded that there is a matching of the slab and soil displacements, except at the slab edge for the two cases that have no loss of contact (Cases A and B). In these two cases the tip of the slab is noted to puncture through the soil mass, which is inconsistent with the displacement compatibility condition expected in similar problems.

To explain this inconsistency, Figure 7.21 shows that a slab loaded with a uniformly distributed load lying on a soft soil behaves differently according to three different subgrade models as shown in Figure 7.21(b),(c),(d). For all the three models there exists full compatibility of the forces, or in otherwords satisfaction of vertical equilibrium. Figure 7.21(b) shows the displacement by a Winkler model where the

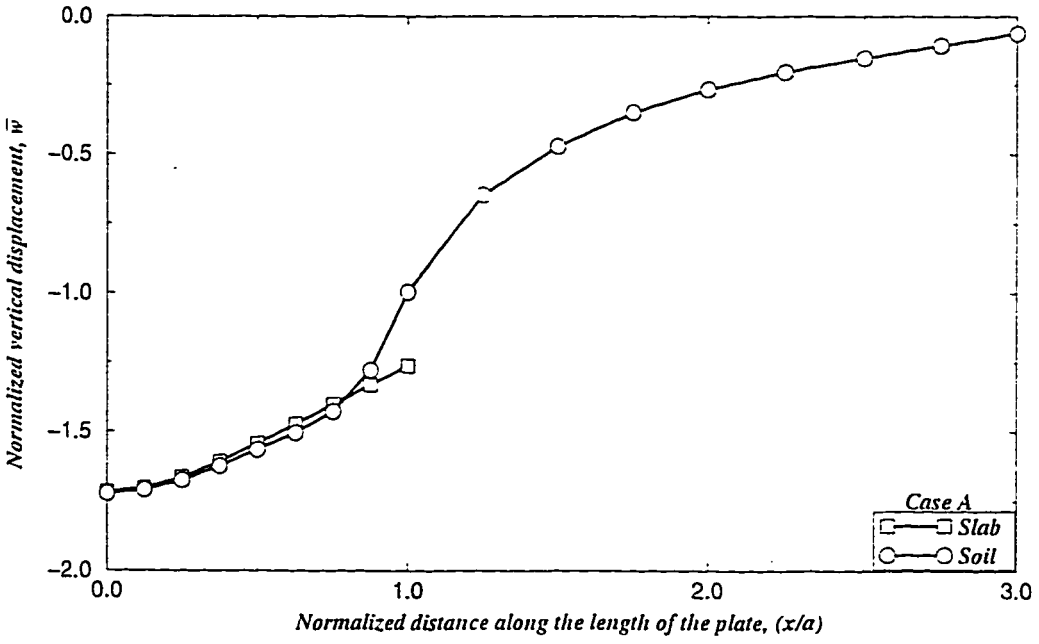

Figure 7.17: Displacement Profile for a Slab Subjected to Patch Loading on a Soft Soil ($\overline{\lambda} = 1.675$).

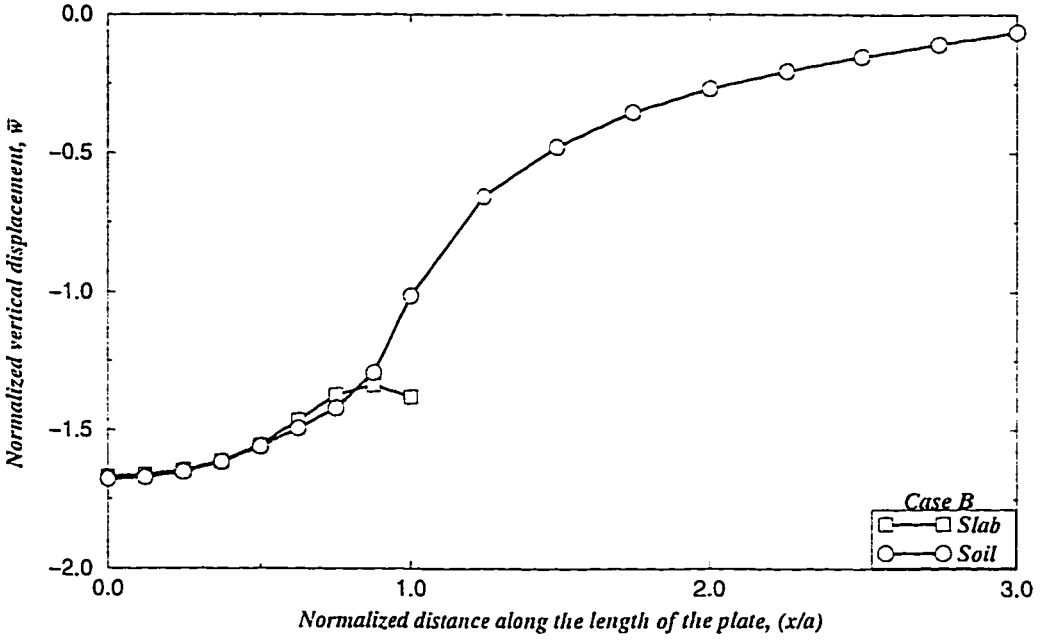

Figure 7.18: Displacement Profile for a Slab Subjected to Uniformly Distributed Load on a Stiff Soil ($\overline{\lambda} = 1675$).

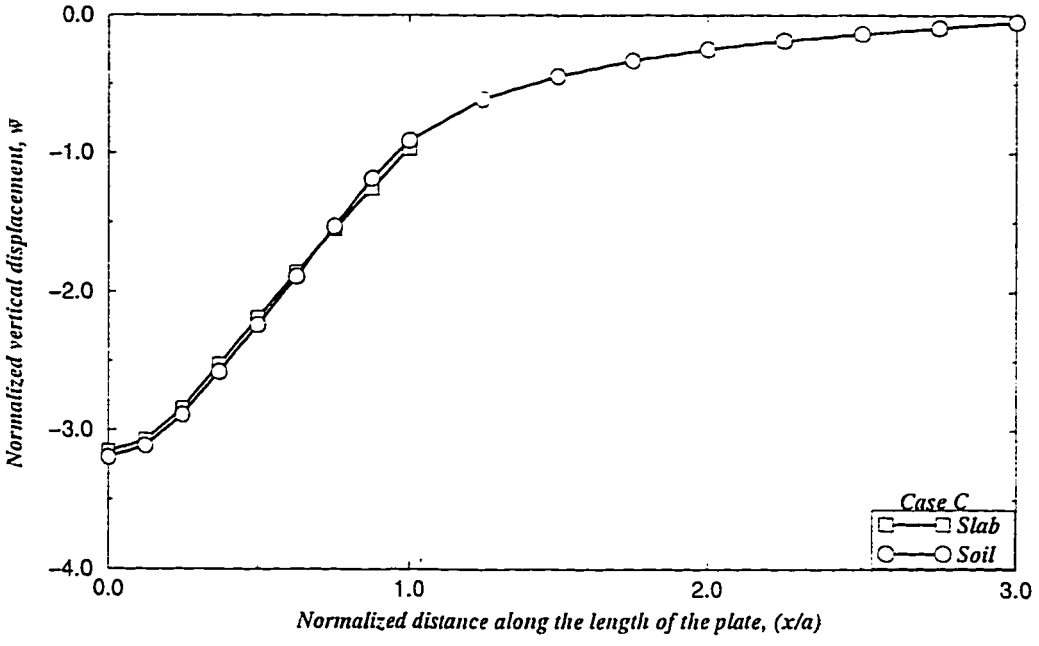

Figure 7.19: Displacement Profile for a Slab Subjected to Patch Loading on an Intermediate Soil ($\overline{\lambda} = 16.75$).

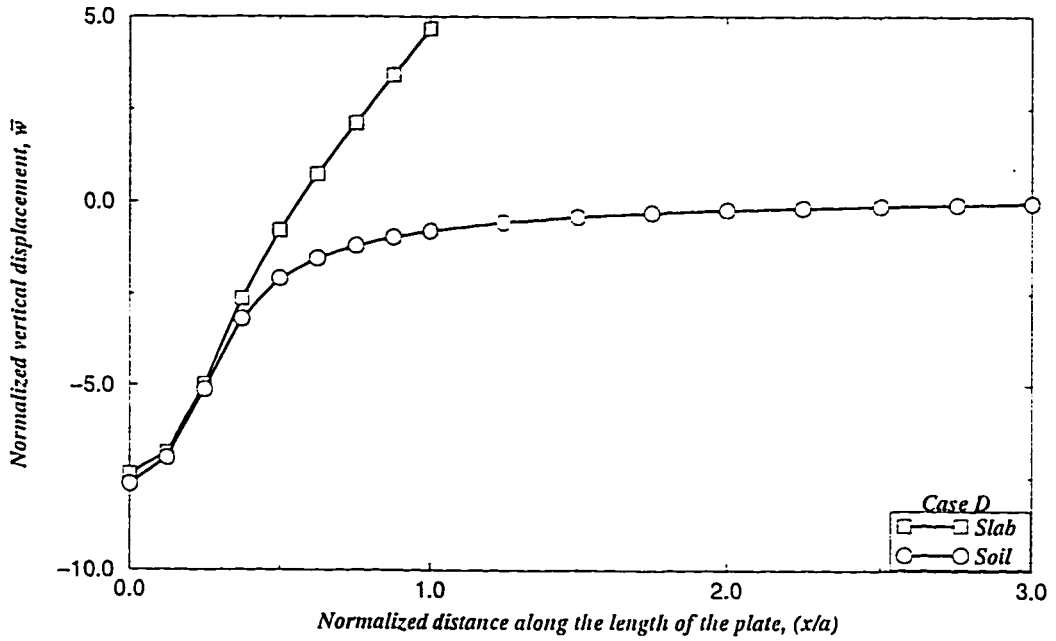

Figure 7.20: Displacement Profile for a Slab Subjected to Patch Loading on a Stiff Soil ($\overline{\lambda} = 1675$).

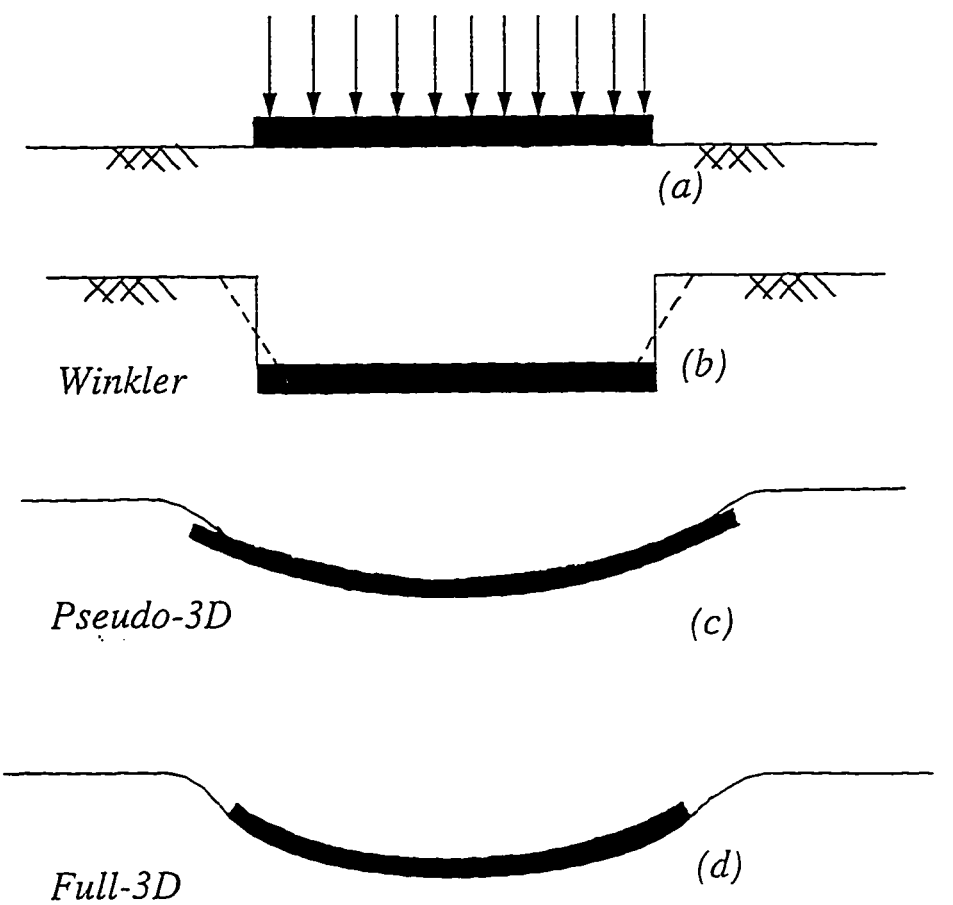

Figure 7.21: Schematic Comparison of Displacement Profiles obtained by Winkler (b), Pseudo-3D (c), and a Full-3D Models.

edge displacements of the slab have no compatibility with that of the soil. For a full three dimensional model the displacements are as shown in Figure 7.21(d), where there exists a full compatibility of both the slab and the soil displacements, which is the realistic behavior of the slab-soil system. Using PSEUDO-3D model the displacements show partial compatibility, and more or less predict the correct behavior at a computational cost only slightly higher than that of Winkler model. On the otherhand, solving the problem with a full-3D analysis increases the computational cost drastically, with relatively little improvement in the results.

7.4.5 Equivalent Subgrade Modulus

Figures 7.22 through 7.25 show the calculated equivalent subgrade modulus obtained using the PSEUDO-3D mode for a slab-soil system, for the four cases explained in Section 7.4.4. These contours are the normalized version of the subgrade reaction values, and involve the parameter α which is given by $\alpha = (2ak)/(E_{soil})$. These curves eliminate the need for the assumption of constant k for a slab on soil and instead show the suggested distributions of k for a more accurate analysis.

From Figure 7.22 and Figure 7.23, it can be concluded that even after increasing the stiffness parameter $\overline{\lambda}$ by 1000 times the contours do not show any significant changes, since there is no loss of contact observed for these two slabs. This means, that as long as the slab is in full contact with the soil there exists a unique α-contour pattern for all loads and all $\overline{\lambda}$ values. However, when the loss of contact behavior

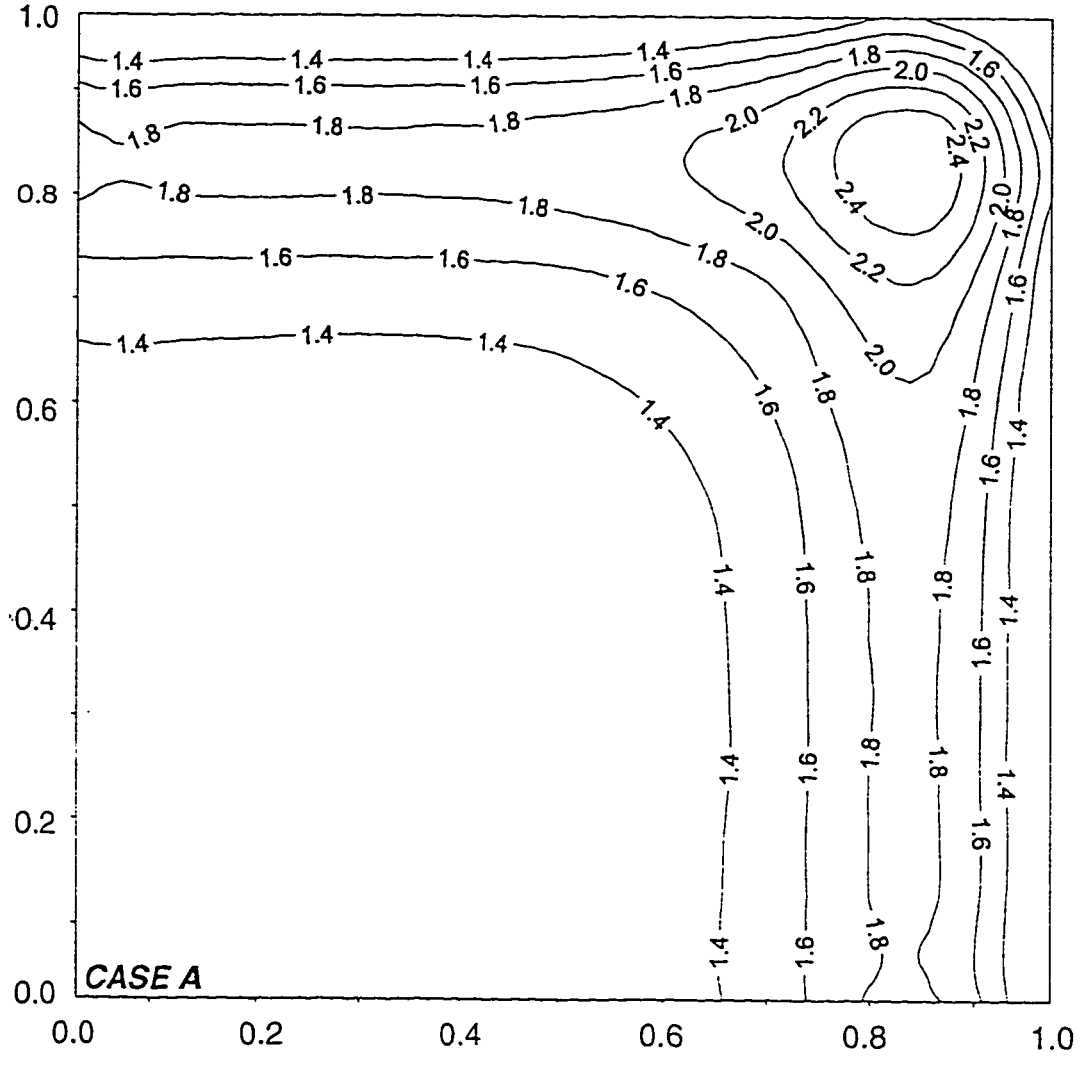

Figure 7.22: Contours of dimensionless relative stiffness parameter α for a slab subjected to patch loading on a weak soil ($\overline{\lambda} = 1.675$).

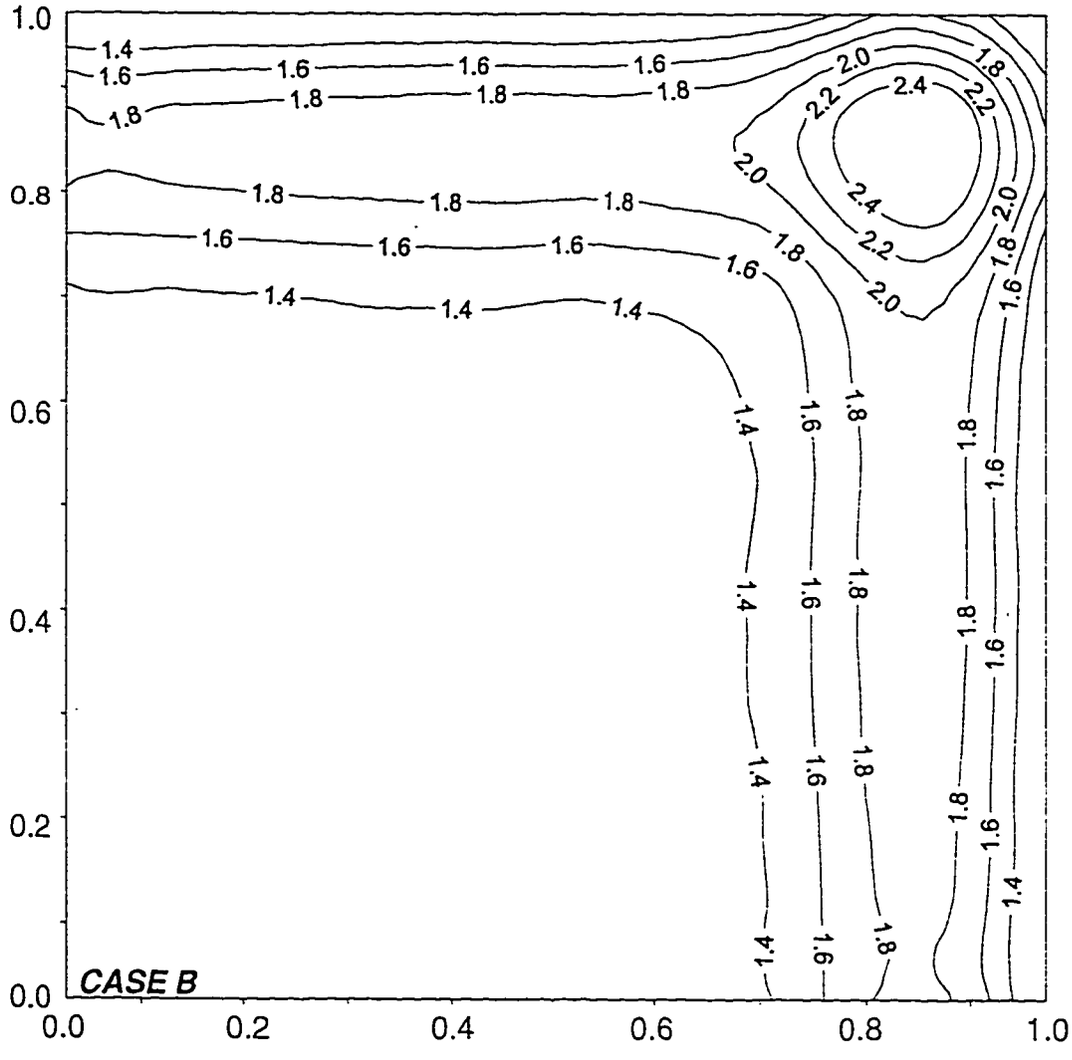

Figure 7.23: Contours of dimensionless relative stiffness parameter α for a slab subjected to uniformly distributed load on a stiff soil ($\overline{\lambda} = 1675$).

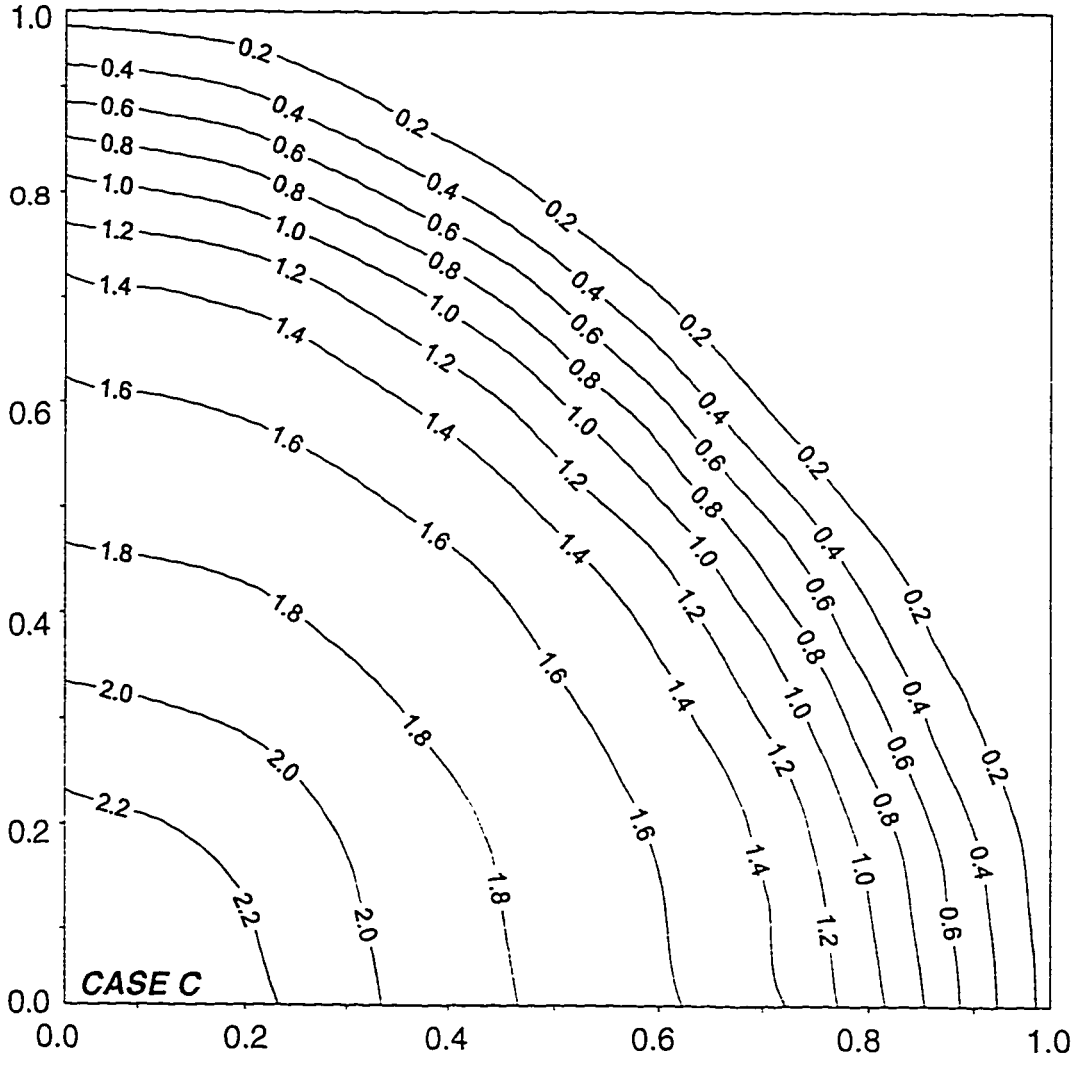

Figure 7.24: Contours of dimensionless relative stiffness parameter α for a slab subjected to patch loading on an intermediate soil ($\overline{\lambda} = 16.75$).

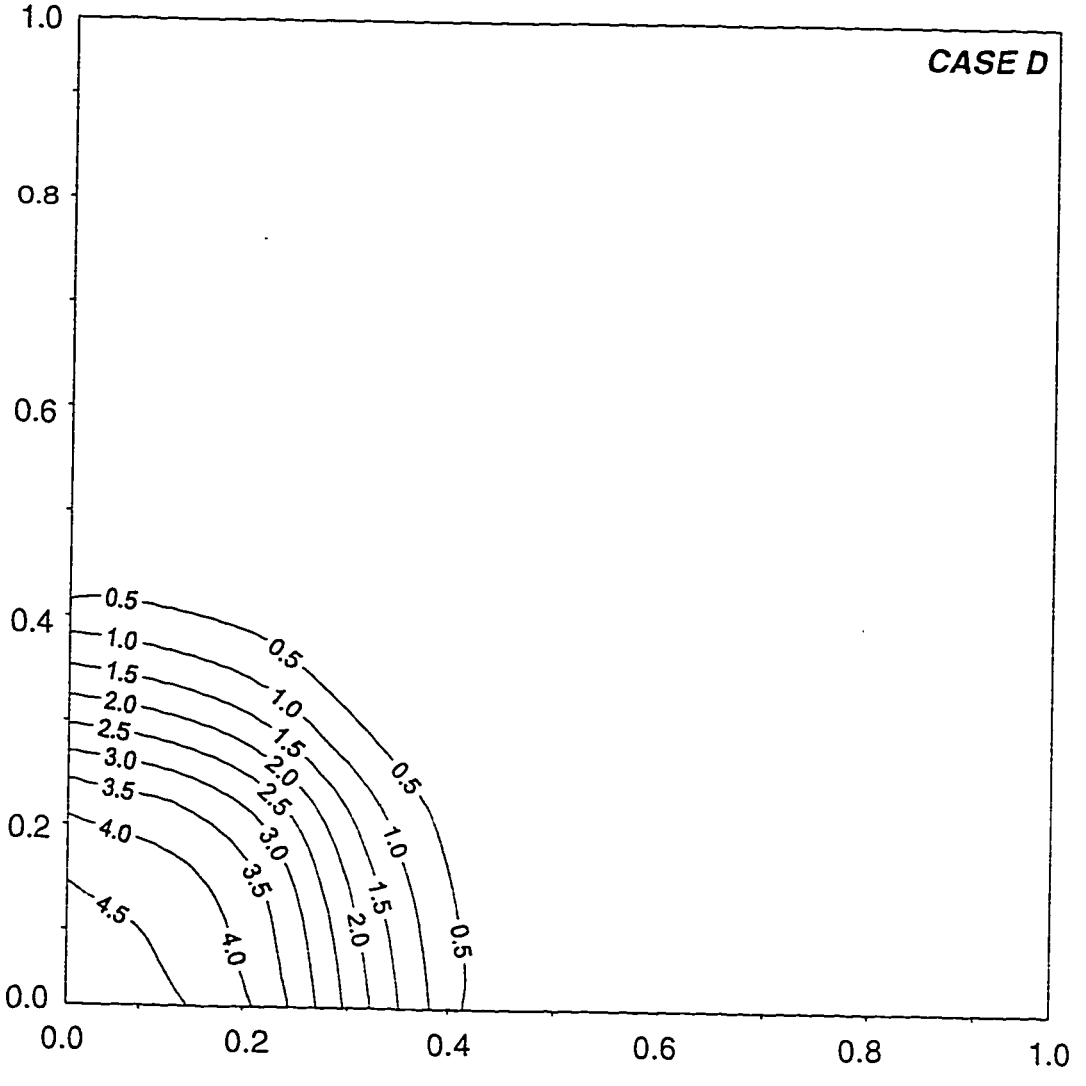

Figure 7.25: Contours of dimensionless relative stiffness parameter α for a slab subjected to patch loading on a stiff soil ($\overline{\lambda} = 1675$).

is experienced then predicting the α value is applicable to each case, since each problem has its own α-contour pattern as shown in Figure 7.24 and Figure 7.25.

7.5 Inelastic Analysis using PSEUDO-3D

7.5.1 Case Description

The square RC slab described in Section 7.3.1, with $h = 80cm$ and two values of $\rho = 0.22\%$ and 0.32%, is analyzed in this section using three different values of E_{soil}. The objective is to study the effect of the soil stiffness E_{soil} on the non-linear behavior of the slab. The effect of the reinforcement ratio on the ultimate loads is also analyzed. Additionally, the load deflection curves and the equivalent subgrade modulus, k-contours, for these cases are presented in the following sections

7.5.2 Non-linear Behavior

In this section, three different soils are used corresponding to weak, intermediate and stiff soils, with each involving two different reinforcement ratios. Figure 7.26 to Figure 7.28 show the non-linear load central deflection curves for $E_{soil} = 10$, 2 and 0.2 kN/cm^2 respectively, for both reinforcement ratios. Table 7.3 gives a summary of ultimate loads for the three selected cases for the inelastic analysis of PSEUDO-3D model. The difference in the ultimate load prediction for the two reinforcement ratios for $E_{soil} = 10$ kN/cm^2 is about 13% whereas for $E_{soil} = 2$ and 0.2 kN/cm^2

Table 7.3: Ultimate Loads for Weak, Intermediate and Stiffer Soils for $\rho = 0.22\%$ and 0.32%

E_{soil} (kN/cm^2)	ρ	
	$\rho = 0.22\%$	$\rho = 0.32\%$
10	P_u=8200kN	P_u=9300kN
2	P_u=5460kN	P_u=7000kN
0.2	P_u=5340kN	P_u=7300kN

they are approximately 21% and 26%, respectively. In addition, as the soil stiffness decreases the central displacements expectedly increase.

The capacity of a slab on a soil, with $E_{soil} = 10\ kN/cm^2$ when compared to a soil with $E_{soil} = 2\ kN/cm^2$ shows a significant difference. However, this difference reduces as the stiffness of soil decreases. From Table 7.3 it can be concluded that below a particular value of E_{soil}, i.e., critical value, the values of the ultimate loads show only little dependence on the soil stiffness.

Table 7.4 gives the load values necessary to produce 1"(2.54 cm) settlement of the slab for the three cases considered. The table shows that the value of P corresponding to 1" settlement is obviously related to E_{soil}, and is almost independent of the reinforcement ratio ρ. The reason is that for $E_{soil} = 2$ and $0.2\ kN/cm^2$ this settlement takes place within the elastic range of the slab.

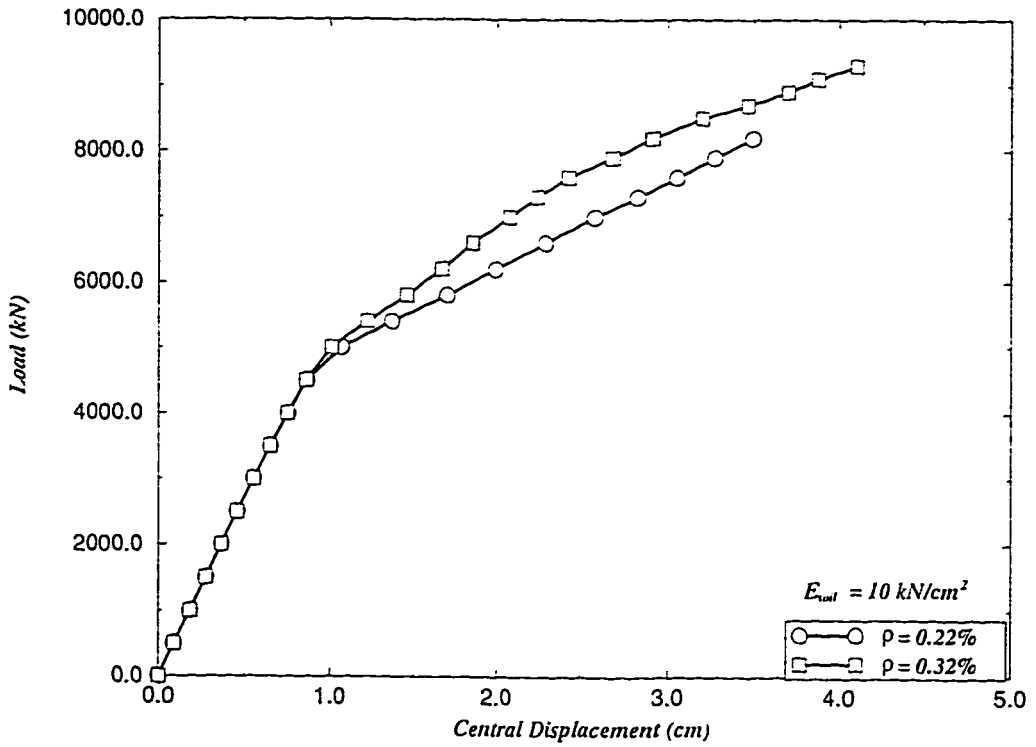

Figure 7.26: Load - Central Deflection Curve for a Slab on a Soil with $E_{soil} = 10kN/cm^2$.

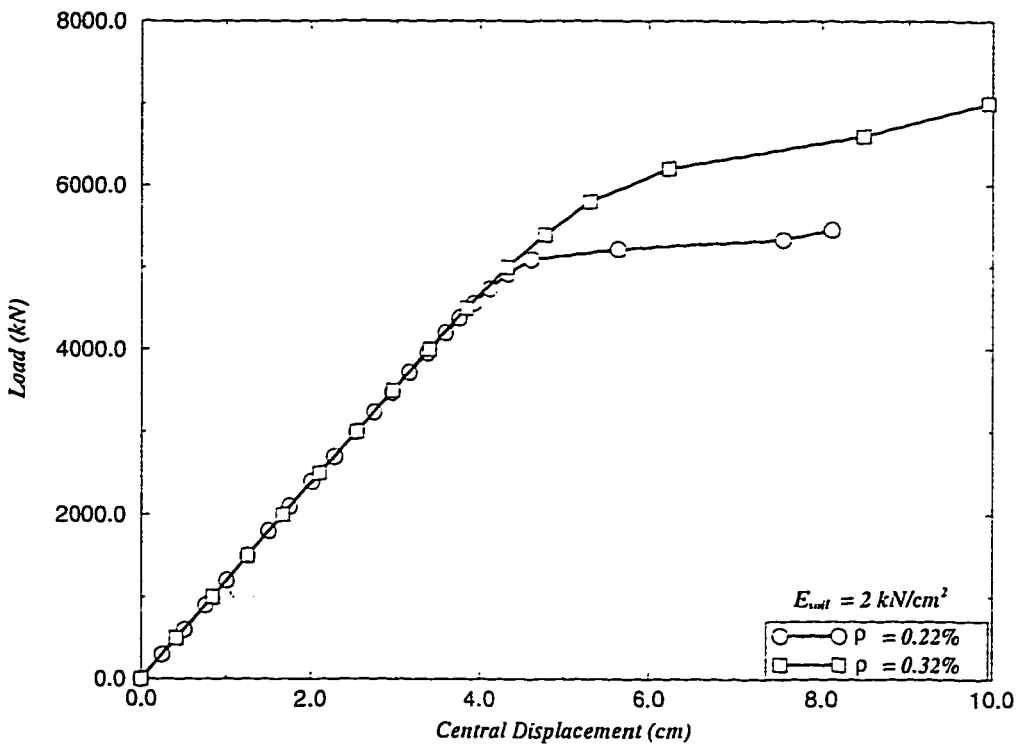

Figure 7.27: Load - Central Deflection Curve for a Slab on a Soil with $E_{soil} = 2kN/cm^2$.

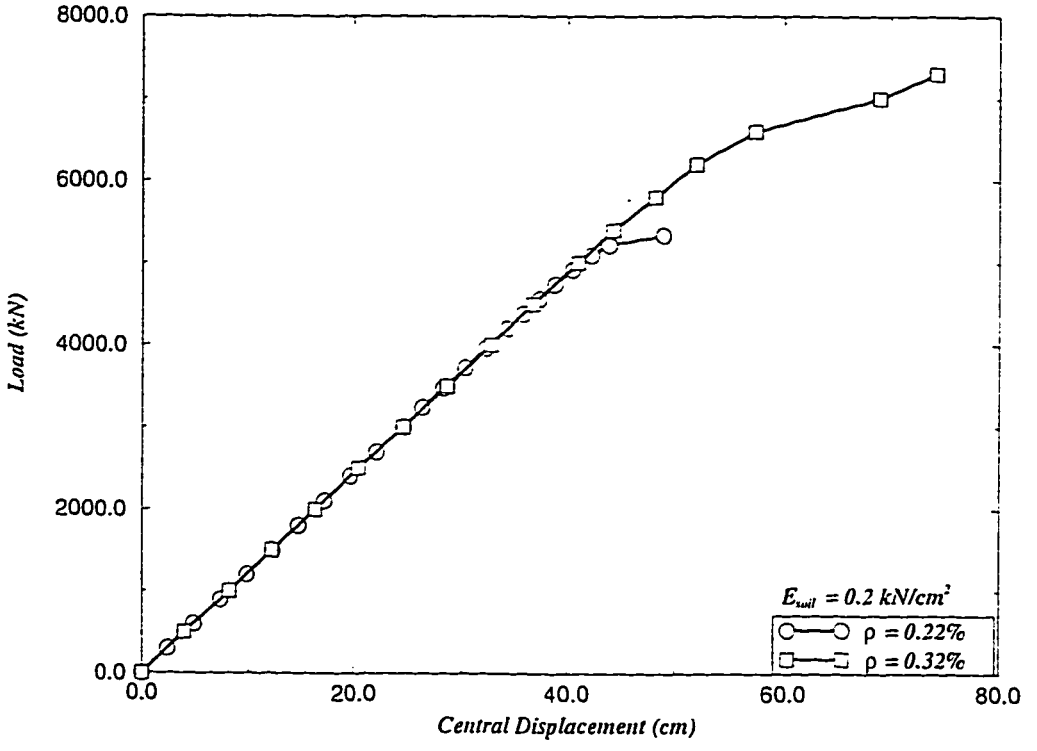

Figure 7.28: Load - Central Deflection Curve for a Slab on a Soil with $E_{soil} = 0.2kN/cm^2$.

Table 7.4: Load corresponding to 1" settlement for Weak, Intermediate and Stiffer Soils for $\rho = 0.22\%$ and 0.32%

E_{soil} (kN/cm^2)	*Load corresponding to 1" settlement*	
	$\rho = 0.22\%$	$\rho = 0.32\%$
10	6950kN	7800kN
2	3000kN	3000kN
0.2	250kN	250kN

7.5.3 Equivalent Subgrade Modulus

Figure 7.29 and Figure 7.30 shows the equivalent subgrade modulus k-contours for a soil with $E_{soil} = 2$ and $10\ kN/cm^2$ respectively at four different load levels. For $E_{soil} = 2\ kN/cm^2$, Figure 7.29 shows that the k-contours do not show any significant change with the increase in load except at the ultimate load. At the ultimate load of $P = 7000kN$, the maximum value of k shifts from the corner towards the center. This shifting in the calculated values of the equivalent subgrade modulus is an interesting phenomenon that confirms the major drawback of the Winkler model. The results shown in Figure 7.29 confirm that not only a variable value of k is needed throughout the slab domain, but it also will change as inelastic deformations develop in the slab due to degradation in concrete and yielding of steel. These non-linearities cause a reduction in the slab rigidity D and are thus reflected in the system stiffness parameter $\overline{\lambda}$.

This phenomenon is illustrated much clearly in Figure 7.30, which is for the stiffer soil ($E_{soil} = 10kN/cm^2$). In this case, it is noted that significant changes in

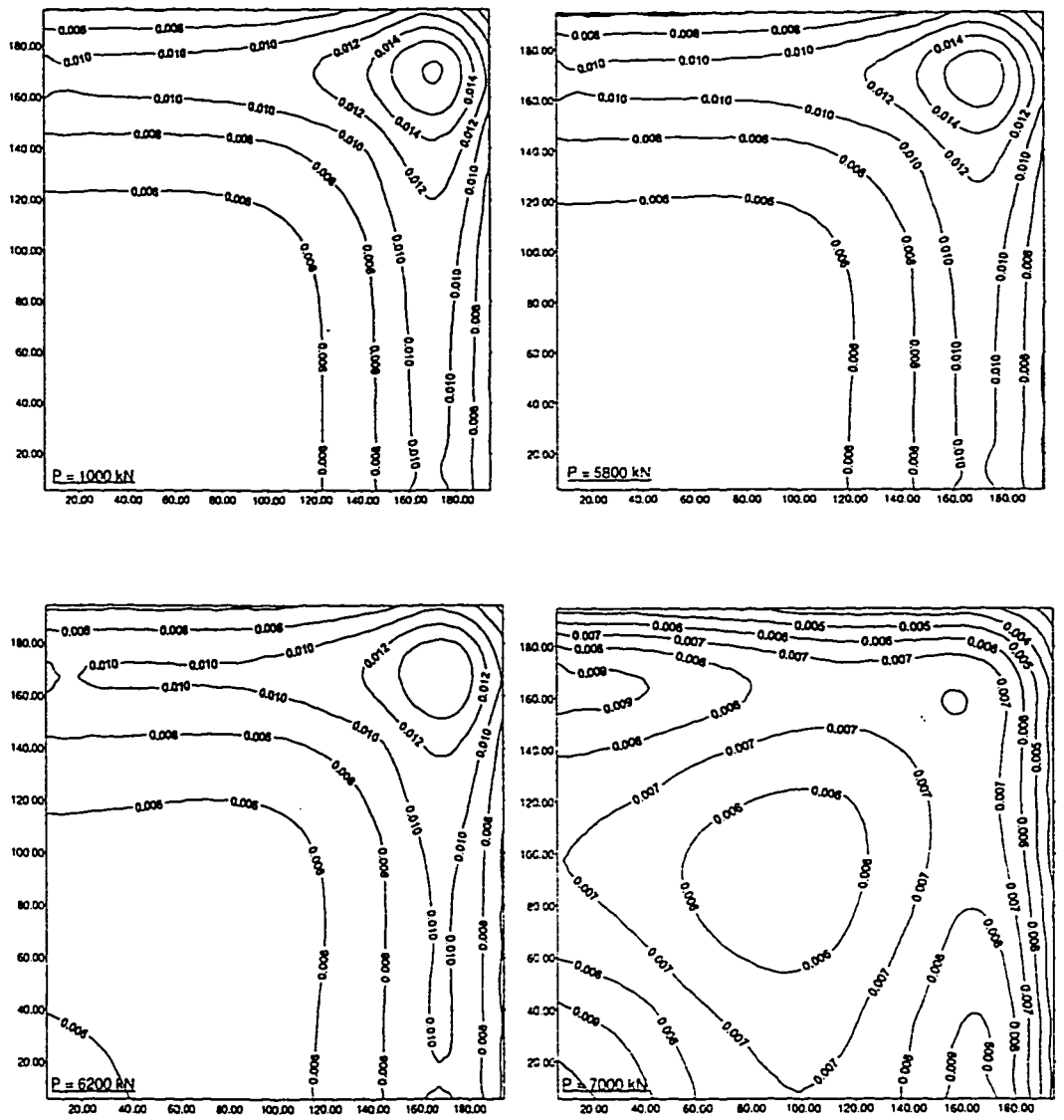

Figure 7.29: Contours of the Equivalent Subgrade Modulus for a Soil with $E_{soil} = 2kN/cm^2$ at Four Different Loads.

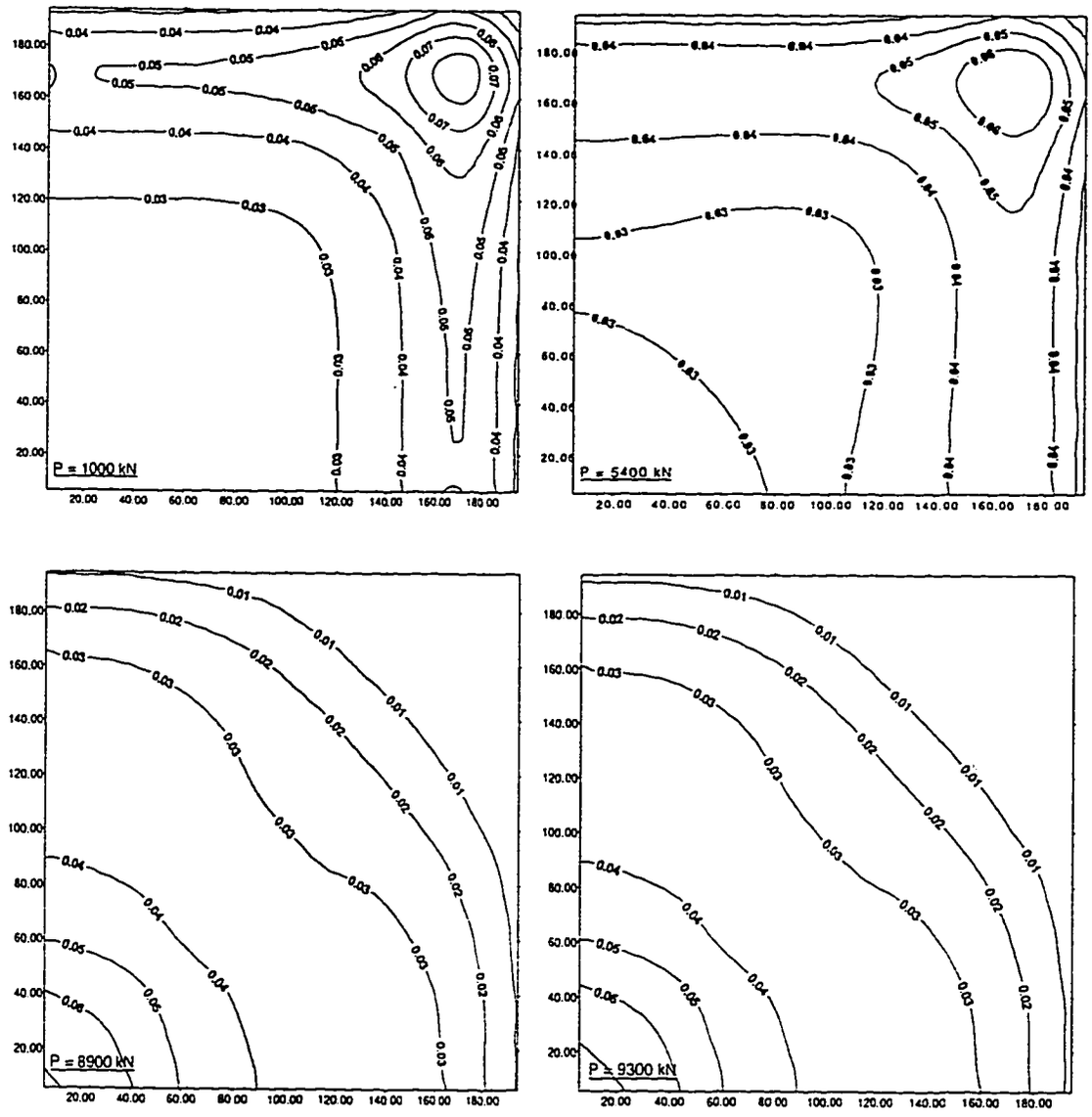

Figure 7.30: Contours of the Equivalent Subgrade Modulus for a Soil with $E_{soil} = 10kN/cm^2$ at Four Different Loads.

the equivalent subgrade modulus values are observed at a load level equal to half the ultimate load of the slab. Further increase in the applied load, will produce equivalent subgrade modulus distributions with loss of contact behavior, similar to Case C described in Section 7.4.4. (Figure 7.24).

Chapter 8

SUMMARY, CONCLUSIONS AND RECOMMENDATIONS

8.1 Summary

To analyze the linear and nonlinear response of slabs on tensionless elastic subgrade, two numerical models, namely, WINKLER and PSEUDO-3D were developed. WINKLER is based on the Winkler's hypothesis whereas PSEUDO-3D is based on a three dimensional elastic analysis. The size effect as well as the location effect of cavities on the behavior of a slab is studied. PSEUDO-3D gives the contours of dimensionless subgrade modulus in the elastic range and contours of subgrade modulus in the inelastic range. The two numerical models, WINKLER and PSEUDO-3D, are compared and contrasted.

8.2 Conclusions

The main conclusions of this work are as follows:

1. A study of slabs resting on tensionless elastic subgrade is made by developing two numerical models, namely, WINKLER and PSEUDO-3D, which use two different approaches to model the soil.

2. The elastic as well as the inelastic behavior of the slab using the proposed model WINKLER is verified by comparing the results to that of Villaggio [11] and Richart [27], respectively. The results show excellent agreement, thus validating the numerical approach employed.

3. The cavity size effect study shows the critical nature of cavity size in predicting the capacity of the slab over a cavity. As long as the cavity size is less than the loaded area, it does not effect the capacity of the slab significantly. But once the size of the cavity increases beyond the loaded area the capacity of the slab is greatly reduced and becomes less than the ACI design value. In addition, as the cavity size increases the mode of failure of the slab changes from a flexural type failure to a punching shear failure.

4. The cavity location effect is studied by analyzing a slab on a soft subgrade (k = 0.01 kN/cm^3) as well as on a stiff subgrade (k = 0.1 kN/cm^3). For the soft subgrade, the cavity location does not show much effect on the capacity of the

slab, whereas for the stiff subgrade a significant effect is seen on the capacity of the slab. The redistribution of pressure uniformly all over the contact area for the soft subgrade and concentration of pressure towards the centre for the stiffer subgrade, contributes to the effect of the cavity location on the capacity of the slab. Additionally, the loss of contact behavior is more predominant for the stiff subgrade case compared to the soft subgrade.

5. The proposed Pseudo-3D model uses an iterative approach to calculate equivalent subgrade modulus values for the slab domain. These values which are similar to the subgrade modulus in Winkler model, are variable and yield more accurate results. The approach was found to be stable and convergent, and can serve as a substitute to the numerically expensive full 3-D analysis.

6. Analyzing a slab by PSEUDO-3D and WINKLER models rightly justifies the advantages of PSEUDO-3D in predicting the realistic behavior of the slab displacements and the contact zone because of its unique solution. Whereas the results from WINKLER model shows the sensitivity of the model to a selected value of subgrade reaction, k, in predicting the slab displacements and the contact zone.

7. The PSEUDO-3D model is tested for a slab on a weak, intermediate, and stiff soils to study the elastic response of the model. Comparing the contours of non-dimensional equivalent subgrade modulus parameter, α, for these three

cases does not show any significant changes, unless there is a loss of contact behavior. Therefore, as long as the slab is in full contact with the soil there exists a unique α-contour pattern for all loads and all soil stiffness values.

8. Three different soils, corresponding to weak ($E_{soil} = 0.2\ kN/cm^2$), intermediate ($E_{soil} = 2\ kN/cm^2$), and stiff ($E_{soil} = 10\ kN/cm^2$) soils are used to study the non-linear behavior of a slab on a soil by PSEUDO-3D model. The capacity of the slab on a stiff soil shows much difference in comparison to the capacity of the slab on a weak soil. This difference ceases to exist for a particular value of E_{soil}, below which decreasing E_{soil} does not have any effect on the slab capacity.

9. The equivalent subgrade modulus k-contours, at different load levels, for a soil with $E_{soil} = 2\ kN/cm^2$, do not show any significant change with the increase in the load except at the ultimate load. Whereas for a soil with $E_{soil} = 10\ kN/cm^2$, this change is seen at an earlier stage of load, equal to half the ultimate load of the slab. The shifting of the equivalent subgrade modulus, k, values from the corner towards the center, confirms the major drawback of the Winkler model, which assumes a constant value of k throughout the analysis.

8.3 Recommendations for future studies

1. The two numerical programs, WINKLER and PSEUDO-3D, can be utilized for analyzing different slab geometries as well as for off-center load positions, and multiple loads.

2. By modifying the two programs, the effect of dowel bars connecting the adjacent slabs, on the extent of load relief that can be attained for a slab can be studied.

3. The plastic nature of the soil can be modelled by modifying the three dimensional elastic element of the program PSEUDO-3D to include plasticity.

Bibliography

[1] S.A. Abbasi. *Non-Linear Finite Element Modelling of Reinforced Concrete Slabs.* PhD thesis, King Fahd University of Petroleum and Minerals, Dhahran, Saudi Arabia, 1991.

[2] G.V. Fernando, M.D. Kotsovos, and M.N. Pavlovic. Symmetrical punching of reinforced concrete slabs: An analytical investigation based on nonlinear finite element modeling. *ACI Structural Journal*, pages 241–250, May-June 1988.

[3] C. Channakeshava and K.T. Sundara Raja Iyengar. Elasto-plastic cracking analysis of reinforced concrete. *Journal of Transportation Engineering*, 114(11):2421–2438, November 1988.

[4] P.M. Lewinski and W. Wojewodzki. Integrated finite element model for reinforced concrete slabs. *Journal of Structural Engineering*, 117(4):1017–1038, April 1991.

[5] V. Huria, K.L. Lee, and A. Emin Aktan. Nonlinear finite element analysis of

reinforced concrete slab bridge. *Journal of Structural Engineering*, 119(1):88-107, January 1993.

[6] H.M. Marzouk and Z. Chen. Finite element analysis of high-strength concrete slabs. *ACI Structural Journal*, 90(5):505-513. September-October 1993.

[7] E. Winkler. Die lehre von der elasticitat und festigkeit. *Prage Dominicus*, 1867.

[8] V.Z. Vlasov and N.N. Leont'ev. Beams, plates and shells on elastic foundations. *Israel Program for Scientific Translations*, 1966.

[9] C.V. Girija Vallabhan, W. Thomas Straughan, and Y.C. Das. Refined model for analysis of plates on elastic foundations. *Journal of Engineering Mechanics*, 117(12):2830-2844, December 1991.

[10] A.M. Ioannides. Finite difference solution for plate on elastic solid. *Journal of Transportation Engineering*, 114(1):57-75, January 1988.

[11] P. Villaggio. A free boundary value problem in plate theory. *Journal of Applied Mechanics*, 50:297-302, June 1983.

[12] Z. Celep. Rectangular plates resting on tensionless elastic foundation. *Journal of Engineering mechanics*, 114(12):2083-2092, December 1988.

[13] A.A. Khathlan and H.A. Waly. Nonaxisymmetric unbonded contact of plates on tensionless winkler foundations. *Mechanics of Structures and Machines*, 22(3):263-281, 1994.

[14] G.G. Meyerhof and K.S.S. Rao. Collapse load of reinforced concrete footings. *Journal of the Structural Division, ASCE.* 100(ST5):1001 1018, May 1974.

[15] D.H. Jiang. Flexural strength of square spread footing. *Journal of Structural Engineering,* 109(8):1812–1819, August 1983.

[16] K.S. Subba Rao and S. Singh. Concentrated load-carrying capacity of concrete slabs on ground. *Journal of Structural Engineering,* 112(12):2628–2645, December 1986.

[17] Y.T. Chou. Stress analysis of small concrete slabs on grade. *Journal of Transportation Engineering,* 110(5):481–492, September 1984.

[18] Y.T. Chou. Subgrade contact pressures under rigid pavements. *Journal of Transportation Engineering,* 109(3):363–379, May 1983.

[19] A. Losberg. Pavements and slabs on grade with structurally active reinforcement. *ACI Journal,* pages 647–657, December 1978.

[20] R.A. Baumann and F.E. Weisgerber. Yield-line analysis of slabs-on-grade. *Journal of Structural Engineering,* 109(7):1553–1568, July 1983.

[21] M. Al-Nasra and L.R.L. Wang. Parametric study of slab-on-grade problems due to intial warping and point loads. *ACI Structural Journal,* 91(1):198-210, March-April 1994.

[22] T. Nogami and Y. C. Lam. Two-parameter layer model for analysis of slab on elastic foundation. *Journal of Engineering Mechanics*. 113(9):1279-1291, September 1987.

[23] A.M. Ioannides and J.P. Donnelly. Three-dimensional analysis of slab on stress-dependent foundation. *Transportation Research Record*, 1196:72-84, 1988.

[24] Y. Kitamura S. Sakurai and N. Shimizu. Three-dimensional elasto-plastic analysis of structure foundation by means of integral equation method. *Proceedings of Conference on Numerical Methods in Geomechanics*, 3:1233-1239, 1982.

[25] C. Channakeshava, F. Barzegar, and G.Z. Voyiadjis. Non-linear finite element analysis of plain concrete pavements with doweled joints. *Journal of Transportation Engineering*, 119(5):763-781, September-October 1993.

[26] M. Sargious and S.K. Wang. Rigid pavement design charts based on a finite element analysis. *Roadways and Airport Pavements, ACI Pubclications SP-51*, pages 33-49, 1975.

[27] F.E. Richart and P. Zia. Effect of local loss of support on foundation design. *Journal of the Soil Mechanics and Foundations Division*, 88(SM 1):1-27, February 1962.

[28] D.H. Jiang and J.H. Shen. Stength of concrete slabs in punching shear. *Journal of the Structural Division, ASCE*. 112(12):2578-2591, December 1986.

[29] E. Hinton and D.R.J. Owen. *Finite Element Software for Plates and Shells.* Pineridge Press, Swansea, U.K., 1984.

[30] E. Hinton and D.R.J. Owen. *Finite Elements in Plasticity Theory and Practice.* Pineridge Press, Swansea, U.K., 1980.

[31] F.E. Richart. Reinforced concrete wall and column footings - part 1. *Journal of the American Concrete Institute*, 20(2):97–127, October 1948.

Vita

- Mansoor Ali Beg
- Hailed from Hyderabad, Andhra Pradesh, India.
- Received Bachelor's degree in Civil Engineering from Osmania University, Hyderabad, India in June, 1992.
- Joined Department of Civil Engineering at King Fahd University of Petroleum and Minerals, Dhahran, Saudi Arabia, as a Research Assistant in February, 1993.
- Completed Master's degree requirements at King Fahd University of Petroleum and Minerals, Dhahran, Saudi Arabia in July, 1996.
- Hobbies include playing Tennis and Cricket, watching T.V., and reading magazines.